



New indolesulfonamide derivatives targeting the colchicine site of tubulin: synthesis, anti-tumour activity, structure–activity relationships, and molecular modelling

Alba Vicente-Blázquez, Myriam González, Manuel Medarde, Faustino Mollinedo & Rafael Peláez

To cite this article: Alba Vicente-Blázquez, Myriam González, Manuel Medarde, Faustino Mollinedo & Rafael Peláez (2021) New indolesulfonamide derivatives targeting the colchicine site of tubulin: synthesis, anti-tumour activity, structure–activity relationships, and molecular modelling, *Journal of Enzyme Inhibition and Medicinal Chemistry*, 36:1, 2025-2044, DOI: [10.1080/14756366.2021.1975277](https://doi.org/10.1080/14756366.2021.1975277)

To link to this article: <https://doi.org/10.1080/14756366.2021.1975277>



© 2021 The Author(s). Published by Informa UK Limited, trading as Taylor & Francis Group.



[View supplementary material](#)



Published online: 12 Sep 2021.



[Submit your article to this journal](#)



Article views: 220



[View related articles](#)



[View Crossmark data](#)

RESEARCH PAPER



New indolesulfonamide derivatives targeting the colchicine site of tubulin: synthesis, anti-tumour activity, structure–activity relationships, and molecular modelling

Alba Vicente-Blázquez^{a,b,c,d}, Myriam González^{a,c,d}, Manuel Medarde^{a,c,d}, Faustino Mollinedo^b and Rafael Peláez^{a,c,d}

^aLaboratorio de Química Orgánica y Farmacéutica, Departamento de Ciencias Farmacéuticas, Universidad de Salamanca, Salamanca, Spain;

^bLaboratory of Cell Death and Cancer Therapy, Department of Molecular Biomedicine, Centro de Investigaciones Biológicas Margarita Salas, Consejo Superior de Investigaciones Científicas (CSIC), Madrid, Spain; ^cFacultad de Farmacia, Instituto de Investigación Biomédica de Salamanca (IBSAL), Universidad de Salamanca, Salamanca, Spain; ^dFacultad de Farmacia, Centro de Investigación de Enfermedades Tropicales de la Universidad de Salamanca (CIETUS), Universidad de Salamanca, Salamanca, Spain

ABSTRACT

Searching for improved indolesulfonamides with higher polarities, 45 new analogues with modifications on the sulfonamide nitrogen, the methoxyaniline, and/or the indole 3-position were synthesised. They show submicromolar to nanomolar antiproliferative IC₅₀ values against four human tumour cell lines and they are not P-glycoprotein substrates as their potencies against HeLa cells did not improve upon cotreatment with multidrug resistance (MDR) inhibitors. The compounds inhibit tubulin polymerisation *in vitro* and in cells, thus causing a mitotic arrest followed by apoptosis as shown by cell cycle distribution studies. Molecular modelling studies indicate binding at the colchicine site. Methylated sulfonamides were more potent than those with large and polar substitutions. Amide, formyl, or nitrile groups at the indole 3-position provided drug-like properties for reduced toxicity, with Polar Surface Areas (PSA) above a desirable 75 Å². Nitriles **15** and **16** are potent polar analogues and represent an interesting class of new antimetotics.

ARTICLE HISTORY

Received 3 June 2021
Revised 11 August 2021
Accepted 14 August 2021



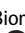
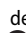
KEYWORDS


Indolesulfonamides; antimetotic; total polar surface area; structure–activity relationships; colchicine-site

Introduction

Microtubules are highly dynamic polymers built up by the lateral association of protofilaments formed by the longitudinal assembly of α,β -tubulin dimers¹. The dynamic assembly and disassembly of the microtubules have critical roles in cell division, vesicle transport, or cytoskeleton-provided cell shape. Therefore, interfering with microtubule dynamics for cancer treatment has gathered increasing interest within the last decades. Seven binding pockets for exogenous ligands have been characterised within the structure of the tubulin dimer or the microtubule lattice to date², encompassing microtubule-stabilizing agents (MSAs), such as paclitaxel, and microtubule-destabilizing agents (MDAs) as well, such as the vinca alkaloids or colchicine. Both groups converge in microtubule dynamics disruption¹. This interference hinders the establishment of proper amphitelic kinetochore-mitotic spindle attachments during metaphase, leading to a sustained G₂/M arrest that can last even days and is somehow linked to the induction of apoptosis^{3,4}. Besides, tubulin sequence alterations are extremely unusual in tumour patients⁵ and some colchicine-site ligands also act as vascular disrupting agents (VDAs) at lower concentrations than those needed to kill tumour cells⁶.

The colchicine site of tubulin is a hydrophobic region located at the interface between the α and β subunits⁷. Bound ligands prevent the transition of the tubulin dimer between the curved and the straight conformation required for polymerisation. Multiple co-crystalline X-ray structures of colchicine site ligands with curved tubulin have led to a better understanding of the domain, which is usually divided into three subpockets (called zones 1–3), although most of them bind only to zones 1 and 2 in a *cisoid* conformation^{2,8}. Combretastatin A-4 (CA-4, **I**), a *cis* stilbene isolated from *Combretum caffrum*, is one of the most promising representatives that has been recently approved for clinical use as its phosphate prodrug fosbretabulin (CA-4P, **II**) (Figure 1)⁹. Due to its high potency, its structure summarises the essential pharmacophoric features for colchicine binding site inhibitors binding at zones 1 and 2: two aromatic non-coplanar rings (A and B), often with methoxy substituents, bound by linkers of different length (0–4 atoms) and nature. The phenylsulfonamide ABT-751 (**IV**) emerged as an orally bioavailable alternative, but it was less effective *in vivo*^{10–14}. Multiple sulfonamide-based ligands with A- and B-ring modifications have thereafter been studied, with varied B rings such as *p*-methoxyphenyls, indoles, benzimidazoles, indazoles, carbazoles, or carbolines². Indolesulfonamides A-293620 (**IX**

CONTACT Faustino Mollinedo  fmollin@cib.csic.es  Laboratory of Cell Death and Cancer Therapy, Department of Molecular Biomedicine, Centro de Investigaciones Biológicas Margarita Salas, Consejo Superior de Investigaciones Científicas (CSIC), Madrid E-28040, Spain; Rafael Peláez  pelaez@usal.es  Laboratorio de Química Orgánica y Farmacéutica, Departamento de Ciencias Farmacéuticas, Universidad de Salamanca, Campus Miguel de Unamuno, Salamanca E-37007, Spain.

 Supplemental data for this article can be accessed [here](#).

© 2021 The Author(s). Published by Informa UK Limited, trading as Taylor & Francis Group.

This is an Open Access article distributed under the terms of the Creative Commons Attribution-NonCommercial License (<http://creativecommons.org/licenses/by-nc/4.0/>), which permits unrestricted non-commercial use, distribution, and reproduction in any medium, provided the original work is properly cited.

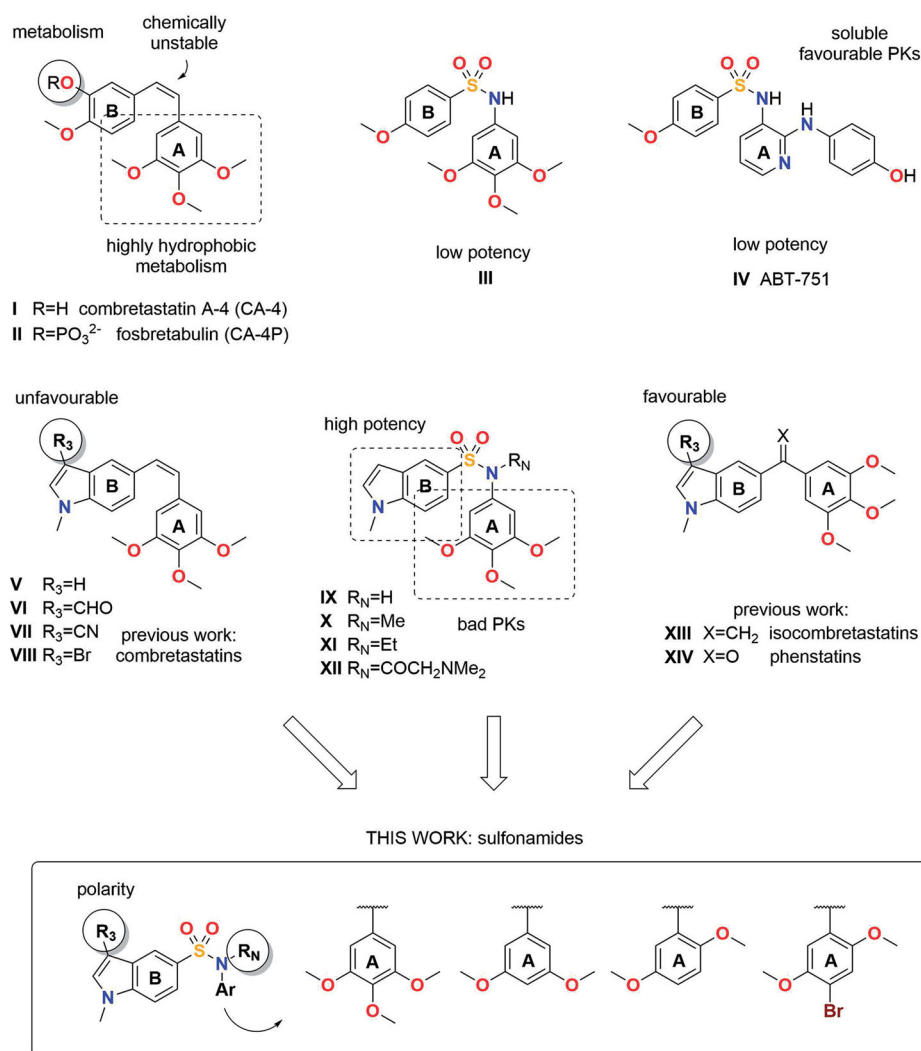


Figure 1. Chemical structure of combretastatins, one-atom bridged derivatives, sulfonamides, and design rationale that led to the compounds reported in this work.

= 4) and its prodrug A-318315 (XII) exerted nanomolar cytotoxic activities against multidrug resistance (MDR)-overexpressing tumour cell lines^{15,16}. We have previously shown that the same replacement of the phenolic B ring of CA-4 (I) by a 1-methyl-5-indolyl moiety in combretastatins (V–VIII)^{17,18} and isocombretastatins (XIII)¹⁹, results in potent anti-tubulin and anti-proliferative activity but worse pharmacokinetics¹⁸. The importance of the 3,4,5-trimethoxyphenyl A ring has also been studied in other sulfonamides with pentafluorophenyl replacements such as T138067 and its prodrug T900607, both of them under ongoing clinical trials^{20–22}, or IG-105^{23,24}, with a 2,6-dimethoxyppyridine. However, most of the attempted modifications improved on the potency at the expense of a more hydrophobic character, as indicated by a reduced Polar Surface Area (PSA), an important predictor of non-specific toxicity and inadequate pharmacokinetics²⁵.

Herein, we have accomplished the synthesis of indolesulfonamides with polar substituents at position 3 to increase the polarity. Different modifications were introduced as well on the sulfonamide nitrogen to explore their effect on potency and pharmacokinetics. Finally, different A rings were explored as replacements for the trimethoxyphenyl ring, which is known to be a point of metabolic transformation²⁶. The effect of the structural modifications on the anti-proliferative activity against several human tumour cell lines has been evaluated. The susceptibility to MDR resistance was assessed by the cytotoxic potency increase in

the presence versus the absence of P-glycoprotein inhibitors. The proposed anti-tubulin mechanism of action was investigated by means of *in vitro* tubulin polymerisation inhibition assays and alteration of the microtubule network in cells, as observed by immunofluorescence microscopy. The apoptotic cell demise was studied by measuring the effects on the cell cycle populations at different time points after treatment. Computational studies have been applied to establish the binding mode of the active ligands with tubulin and to ascertain the physicochemical properties that might result in an improved pharmacokinetic profile. Our results show that indolesulfonamides are potent antimetabolic agents able to inhibit tumour cell proliferation and that polar substitutions at the indole 3-position, such as cyano groups, result in an optimal combination of anti-proliferative potency and polarity that makes them interesting new anti-tumour drugs for further development.

Materials and methods

General chemical techniques

All the solvents and reagents were used as purchased from commercial suppliers without further purification. The solvents were stored over molecular sieves except for THF, which was freshly refluxed with sodium/benzophenone right before use, and hexane, dried by distillation and stored over CaCl₂. Melting points

were measured on a Buchi 510 apparatus, an LLG MPM-HV2 apparatus, or an Electrothermal ET0001 digital melting point apparatus and are uncorrected. NMR spectra were acquired on a Varian Mercury Spectrometer operating at 400/100 MHz for $^1\text{H}/^{13}\text{C}$, respectively. Chemical shift values (δ) are expressed in ppm downfield from tetramethylsilane and coupling constants (J) are given in Hz. A Nicolet Impact 410 Spectrophotometer was used for IR spectra in the KBr disc, and absorption frequencies are expressed in cm^{-1} . A hybrid QSTAR XL quadrupole/time of flight spectrometer was used for HRMS analyses. GC-MS spectra were performed using a Hewlett-Packard 5890 series II mass detector. Reactions were monitored by thin-layer chromatography (TLC) using pre-coated silica gel plates (0.25 mm thickness) with UV fluorescence indicator 254 (Polychrom SI F₂₅₄). Column purifications were carried out using silica gel columns by flash chromatography (Kieselgel 40, 0.040–0.063 mm; Merck), and 1.0 mm thickness silica gel plates were used for preparative TLC purifications (PLC Kieselgel 60 F₂₅₄; concentration zone 20 × 4 cm).

Method A: general procedure for the synthesis of indolinesulfonamides

A room temperature mixture of **1** (1.1 mmol), the corresponding aniline (1.0 mmol), and NaHCO_3 (1.5 mmol) in EtOAc/water (1:1, v/v) was stirred under N_2 atmosphere. Upon completion, the reaction was diluted with 0.5 parts of MTBE and stirred at 4 °C. The suspension was filtered off, and the precipitate was washed with water and MTBE. The product (**2**, **19**, or **33**) was obtained as a mixture of rotamers and used in the next reaction without further purification.

Method B: general procedure for the reduction of N-formylindolines

NaBH_4 (1.5–3.0 mmol) was added to a solution of the *N*-formylindoline derivative (**2**, **19**, or **33**) (1.0 mmol) in THF at 4 °C. Trichloroacetic acid (1.5–3.0 mmol) was subsequently added, and the reaction was warmed to room temperature under N_2 . Upon completion, the solution was three-fold diluted with water and vigorously stirred at 4 °C. The suspension was filtered off, and the precipitate was washed with water and MTBE, providing the product (**3**, **20**, or **34**), used in the next reaction without further purification.

Method C: general procedure for aromatisation of N-methylindolines

DDQ (1.1 mmol) was added to a solution of the *N*-methylindoline derivative (**3**, **20**, or **34**) (1.0 mmol) in THF at 4 °C. The reaction was warmed to room temperature under N_2 . Upon completion, it was concentrated in half the volume, diluted with 1 part of MTBE, and stirred at 4 °C. The suspension was filtered off, and the precipitate was washed with MTBE. Crystallisation from acetonitrile/MTBE provided the product (**4**, **21**, or **35**).

Method D: general procedure for alkylation of sulfonamides

Method D1. The sulfonamide (**4**, **12**, **21**, **35**, **40**, or **45**) (1 mmol) was stirred in acetonitrile with excess KOH for 30 min at room temperature. Then, methyl iodide or ethyl bromide (2 mmol) were added. Upon completion, KOH was filtered off, and the filtrate was evaporated, dissolved in CH_2Cl_2 , and washed with brine. The organic layer was dried over anhydrous Na_2SO_4 , filtered, and

concentrated to dryness. Methylation (**5**, **13**, **22**, **36**, **41**, or **46**) or ethylation (**6**, **14**, or **23**) products were obtained by column chromatography, preparative TLC, or crystallisation.

Method D2. The alkyl halide (2.0–2.4 mmol of ethyl bromoacetate, 2.0–8.6 mmol of chloroacetonitrile, 2.0–2.2 mmol of benzyl chloride, or 2.3 mmol of 4-fluorobenzyl chloride) was added to a solution of the sulfonamide (**4**, **21**, or **35**) (1.0 mmol) in DMF with excess K_2CO_3 and stirred at room temperature. Upon completion, it was filtered and evaporated. The residue was dissolved in CH_2Cl_2 , washed with brine, dried over anhydrous Na_2SO_4 , filtered, and evaporated under vacuum. The products were obtained by column chromatography or crystallisation: ethyl acetate (**7**, **24**, and **37**), acetonitrile (**9**, **25**, and **38**), or benzyl (**26**, **27**, and **39**) derivatives.

Method E: general procedure for brominations

NBS (1.1 or 2.2 mmol) was added to a solution of the sulfonamide (**4**, **6**, **35**, **40**, or **41**) (1.0 mmol) in CH_2Cl_2 at 4 °C. Upon completion, the mixture was evaporated. Crystallisation provided the brominated products (**10**, **11**, **45**, **47**, and **48**).

Method F: general procedure for the formylation of indoles

POCl_3 (6 mmol) was added dropwise to DMF (0.5–2 mL) at 4 °C and stirred for 30 min under N_2 . The mixture was subsequently added drop by drop to a solution of the indole derivative (**4**, **22**, **26**, or **35**) (1 mmol) in DMF (0.5–8 mL) at 4 °C and progressively warmed to room temperature. Upon completion, the reaction was poured into iced water with sodium acetate and kept at 4 °C. The resulting precipitate was filtered off, providing the aldehyde derivative (**12**, **29**, **30**, and **40**), then crystallised from MeOH/acetone or MeOH/ CH_2Cl_2 .

Method G: general procedure for the transformation of aldehydes into nitriles

Method G1. A mixture of the aldehyde (**12**, **13**, **29**, **30**, **40**, or **47**) (1 mmol), $\text{NH}_2\text{OH}\cdot\text{HCl}$ (10 mmol), and 4 drops of pyridine was heated in refluxing methanol. Upon completion, methanol was evaporated and the residue dissolved in CH_2Cl_2 was washed with brine. The organic layer was dried over anhydrous Na_2SO_4 , filtered, and rotary evaporated to obtain a mixture of oximes. That mixture was dissolved in pyridine with excess acetic anhydride and heated at 130 °C under N_2 atmosphere. The reaction was poured onto ice and extracted with CH_2Cl_2 , washed with 2 N HCl, 5% NaHCO_3 , and brine. The organic layer was dried over anhydrous Na_2SO_4 , filtered, and evaporated. Crystallisation from MeOH/acetone gave the indole-3-carbonitrile derivative (**15**, **16**, **31**, **32**, **42**, **43**, and **49**).

Method G2. The aldehyde derivative (**12** or **40**) (1.0 mmol) was stirred with excess KOH in acetonitrile for 30 min. For simultaneous alkylation of the sulfonamide, methyl iodide (4.7 mmol) or ethyl bromide (2.3 mmol) were optionally added. After 6 days, the reaction was evaporated, re-dissolved in CH_2Cl_2 , and washed with brine. The organic layer was dried over anhydrous Na_2SO_4 , filtered, and evaporated. Preparative TLC provided *E* and *Z* propenenitriles (**17E/Z**, **18E/Z**, and **44E/Z**).

Characterisation of compounds

1-Formylindoline-5-sulfonyl chloride (1). Prepared as previously described¹⁶. Yield: 99%. Yellow powder. IR (KBr): 1678, 1494, 1360, 1180 cm⁻¹. ¹H NMR (400 MHz, CDCl₃): δ (E) 3.27 (t, *J* = 8.8 Hz, 2H), 4.17 (t, *J* = 8.8 Hz, 2H), 7.30 (d, *J* = 8.0 Hz, 1H), 7.89 (m, 2H), 9.04 (s, 1H). (Z) 3.32 (t, *J* = 8.4 Hz, 2H), 4.26 (t, *J* = 8.4 Hz, 2H), 7.89 (m, 2H), 8.25 (d, *J* = 8.4 Hz, 1H), 8.58 (bs, 1H). ¹³C NMR (100 MHz, CDCl₃): δ 26.6 (CH₂), 27.3 (CH₂), 45.5 (CH₂), 47.4 (CH₂), 109.3 (CH), 116.4 (CH), 123.9 (CH), 125.2 (CH), 128.4 (CH), 133.8 (C), 139.2 (C), 147.1 (C), 147.3 (C), 157.7 (CH), 160.1 (CH).

1-Formyl-N-(3,4,5-trimethoxyphenyl)indoline-5-sulfonamide (2). Obtained as described in Method A using 3,4,5-trimethoxyaniline. Yield: 83%. White powder. All spectral data are in agreement with those reported in the literature¹⁶.

1-Methyl-N-(3,4,5-trimethoxyphenyl)indoline-5-sulfonamide (3). Obtained as described in Method B from **2**. Yield: 89%. White powder. All spectral data are in agreement with those reported in the literature¹⁶.

1-Methyl-N-(3,4,5-trimethoxyphenyl)-1H-indole-5-sulfonamide (4). Obtained as described in Method C from **3**. Yield: 70%. White powder. All spectral data are in agreement with those reported in the literature¹⁶.

N,1-Dimethyl-N-(3,4,5-trimethoxyphenyl)-1H-indole-5-sulfonamide (5). Obtained as described in Method D1 from **4**¹⁶. Yield: 91%. Yellow solid. IR (KBr): 1594, 1498, 1345, 1157, 644 cm⁻¹. ¹H NMR (400 MHz, CDCl₃): δ 3.12 (s, 3H), 3.67 (s, 6H), 3.84 (s, 3H), 3.85 (s, 3H), 6.28 (s, 2H), 6.52 (d, *J* = 3.2 Hz, 1H), 7.18 (d, *J* = 3.2 Hz, 1H), 7.35 (d, *J* = 8.4 Hz, 1H), 7.44 (dd, *J* = 2.0, 8.4 Hz, 1H), 7.97 (d, *J* = 2.0 Hz, 1H). ¹³C NMR (100 MHz, CDCl₃): δ 33.1 (CH₃), 38.5 (CH₃), 56.1 (2) (CH₃), 60.9 (CH₃), 102.6 (CH), 104.7 (2) (CH), 109.1 (CH), 121.0 (CH), 122.4 (CH), 126.9 (C), 127.6 (C), 131.2 (CH), 137.3 (C), 137.8 (C), 138.4 (C), 152.8 (2) (C). HRMS (C₁₉H₂₂N₂NaO₅S⁺): calcd. 413.1142 (M + Na⁺), found 413.1138.

N-Ethyl-1-methyl-N-(3,4,5-trimethoxyphenyl)-1H-indole-5-sulfonamide (6). Obtained as described in Method D1 from **4**¹⁶. Yield: 84%. Yellow crystals, m.p. (CH₂Cl₂/Hex): 175.9–176.3 °C. IR (KBr): 1595, 1331, 1124, 644 cm⁻¹. ¹H NMR (400 MHz, CDCl₃): δ 1.07 (t, *J* = 7.2 Hz, 3H), 3.53 (q, *J* = 7.2 Hz, 2H), 3.64 (s, 6H), 3.84 (s, 6H), 6.22 (s, 2H), 6.57 (d, *J* = 3.2 Hz, 1H), 7.17 (d, *J* = 3.2 Hz, 1H), 7.35 (d, *J* = 8.4 Hz, 1H), 7.51 (dd, *J* = 1.6, 8.4 Hz, 1H), 7.99 (d, *J* = 1.6 Hz, 1H). ¹³C NMR (100 MHz, CDCl₃): δ 14.1 (CH₃), 33.1 (CH₃), 45.7 (CH₂), 56.0 (2) (CH₃), 60.9 (CH₃), 102.5 (CH), 106.6 (2) (CH), 109.1 (CH), 120.8 (CH), 122.2 (CH), 127.6 (C), 128.6 (C), 131.2 (CH), 135.0 (C), 137.6 (C), 138.3 (C), 152.9 (2) (C). HRMS (C₂₀H₂₅N₂O₅S⁺): calcd. 405.1479 (M + H⁺), found 405.1481.

Ethyl N-((1-methyl-1H-indol-5-yl)sulfonyl)-N-(3,4,5-trimethoxyphenyl)glycinate (7). Obtained as described in Method D2 from **4**. Yield: 91%. Yellow crystals, m.p. (MeOH): 124.5–125.8 °C. IR (KBr): 1750, 1503, 1334, 641 cm⁻¹. ¹H NMR (400 MHz, CDCl₃): δ 1.22 (t, *J* = 7.2 Hz, 3H), 3.48 (s, 6H), 3.81 (s, 3H), 3.84 (s, 3H), 4.15 (q, *J* = 7.2 Hz, 2H), 4.36 (s, 2H), 6.39 (s, 2H), 6.56 (d, *J* = 3.2 Hz, 1H), 7.17 (d, *J* = 3.2 Hz, 1H), 7.35 (d, *J* = 8.8 Hz, 1H), 7.57 (dd, *J* = 1.6, 8.8 Hz, 1H), 8.03 (d, *J* = 1.6 Hz, 1H). ¹³C NMR (100 MHz, CDCl₃): δ 14.1 (CH₃), 33.1 (CH₃), 52.9 (CH₂), 55.9 (2) (CH₃), 60.7 (CH₂), 61.3 (CH₃), 102.5 (CH), 106.4 (2) (CH), 109.2 (CH), 120.6 (CH), 122.2 (CH),

127.5 (C), 129.0 (C), 131.3 (CH), 135.8 (C), 137.7 (C), 138.3 (C), 152.9 (2) (C), 168.9 (C). HRMS (C₂₂H₂₇N₂O₇S⁺): calcd. 463.1533 (M + H⁺), found 463.1522.

N-((1-Methyl-1H-indol-5-yl)sulfonyl)-N-(3,4,5-trimethoxyphenyl)glycine (8). Compound **7** (130 mg, 0.28 mmol) in methanol (5 mL) with excess KOH was vigorously stirred for 30 min, and subsequently concentrated to be dissolved in CH₂Cl₂ and washed with brine. The organic layer was dried over anhydrous Na₂SO₄, filtered, and evaporated. The solid (**8**, 83 mg, 0.19 mmol, 68%) was purified by flash chromatography (CH₂Cl₂/methanol 9:1) to obtain **8** (29 mg, 0.07 mmol, 24%). White solid. IR (KBr): 2943, 1731, 1589, 1129, 649 cm⁻¹. ¹H NMR (400 MHz, CDCl₃): δ 3.58 (s, 6H), 3.77 (s, 3H), 3.80 (s, 3H), 4.34 (s, 2H), 6.35 (s, 2H), 6.53 (d, *J* = 3.2 Hz, 1H), 7.14 (d, *J* = 3.2 Hz, 1H), 7.32 (d, *J* = 8.8 Hz, 1H), 7.53 (dd, *J* = 2.0, 8.8 Hz, 1H), 8.00 (d, *J* = 2.0 Hz, 1H). ¹³C NMR (100 MHz, CDCl₃): δ 33.2 (CH₃), 53.4 (CH₂), 56.0 (2) (CH₃), 60.8 (CH₃), 102.7 (CH), 106.3 (2) (CH), 109.4 (CH), 120.8 (CH), 122.4 (CH), 127.6 (C), 128.7 (C), 131.2 (CH), 135.9 (C), 137.7 (C), 138.4 (C), 153.0 (2) (C), 173.0 (C). HRMS (C₂₀H₂₂N₂NaO₇S⁺): calcd. 457.1040 (M + Na⁺), found 457.1035.

N-(Cyanomethyl)-1-methyl-N-(3,4,5-trimethoxyphenyl)-1H-indole-5-sulfonamide (9). Obtained as described in Method D2 from **4**. Yield: 70%. White crystals, m.p. (CH₂Cl₂/Hex): 140.2–141.0 °C. IR (KBr): 1594, 1342, 1125, 642 cm⁻¹. ¹H NMR (400 MHz, CDCl₃): δ 3.63 (s, 6H), 3.84 (s, 3H), 3.86 (s, 3H), 4.56 (s, 2H), 6.36 (s, 2H), 6.60 (d, *J* = 3.2 Hz, 1H), 7.20 (d, *J* = 3.2 Hz, 1H), 7.41 (d, *J* = 8.8 Hz, 1H), 7.59 (dd, *J* = 2.0, 8.8 Hz, 1H), 8.03 (d, *J* = 2.0 Hz, 1H). ¹³C NMR (100 MHz, CDCl₃): δ 33.2 (CH₃), 39.8 (CH₂), 56.0 (2) (CH₃), 60.9 (CH₃), 102.9 (CH), 106.0 (2) (CH), 109.6 (CH), 115.2 (C), 120.8 (CH), 122.8 (CH), 127.5 (C), 127.7 (C), 131.6 (CH), 134.2 (C), 138.5 (C), 138.7 (C), 153.4 (2) (C). HRMS (C₂₀H₂₂N₃O₅S⁺): calcd. 416.1275 (M + H⁺), found 416.1266.

3-Bromo-1-methyl-N-(3,4,5-trimethoxyphenyl)-1H-indole-5-sulfonamide (10). Obtained as described in Method E from **4**. Yield: 61%. White crystals, m.p. (CH₂Cl₂): 236.9–237.2 °C. IR (KBr): 3247, 1604, 1329, 1127, 1010 cm⁻¹. ¹H NMR (400 MHz, CDCl₃): δ 3.71 (s, 6H), 3.74 (s, 3H), 3.79 (s, 3H), 6.29 (s, 2H), 6.39 (bs, 1H), 7.18 (s, 1H), 7.31 (d, *J* = 8.8 Hz, 1H), 7.61 (dd, *J* = 1.6, 8.8 Hz, 1H), 8.09 (d, *J* = 1.6 Hz, 1H). ¹³C NMR (100 MHz, DMSO-d₆): δ 33.5 (CH₃), 56.1 (2) (CH₃), 60.5 (CH₃), 89.2 (C), 97.9 (2) (CH), 111.8 (CH), 119.1 (CH), 120.8 (CH), 126.1 (C), 131.3 (C), 131.9 (CH), 134.3 (C), 134.5 (C), 138.0 (C), 153.4 (2) (C). HRMS (C₁₈H₁₉BrN₂NaO₅S⁺): calcd. 477.0090 (M + Na⁺), found 477.0091.

3-Bromo-N-ethyl-1-methyl-N-(3,4,5-trimethoxyphenyl)-1H-indole-5-sulfonamide (11). Obtained as described in Method E from **6**. Yield: 78%. Yellow crystals, m.p. (MeOH/CH₂Cl₂): 155.7–156.2 °C. IR (KBr): 1594, 1234, 1128, 647 cm⁻¹. ¹H NMR (400 MHz, CDCl₃): δ 1.09 (t, *J* = 7.2 Hz, 3H), 3.53 (q, *J* = 7.2 Hz, 2H), 3.68 (s, 6H), 3.84 (s, 3H), 3.86 (s, 3H), 6.24 (s, 2H); 7.21 (s, 1H), 7.35 (d, *J* = 8.8 Hz, 1H), 7.56 (dd, *J* = 1.6, 8.8 Hz, 1H), 7.94 (d, *J* = 1.6 Hz, 1H). ¹³C NMR (100 MHz, CDCl₃): δ 14.1 (CH₃), 33.4 (CH₃), 47.8 (CH₂), 56.1 (2) (CH₃), 60.9 (CH₃), 91.0 (C), 106.5 (2) (CH), 109.5 (CH), 120.8 (CH), 122.1 (CH), 126.8 (C), 130.0 (C), 130.1 (CH), 134.8 (C), 137.8 (C), 137.9 (C), 153.0 (2) (C). HRMS (C₂₀H₂₃BrN₂NaO₅S⁺): calcd. 505.0403 (M + Na⁺), found 505.0403.

3-Formyl-1-methyl-N-(3,4,5-trimethoxyphenyl)-1H-indole-5-sulfonamide (12). Obtained as described in Method F from **4**. Yield:

95%. Yellow crystals, m.p. (MeOH/acetone): 237.9–238.3 °C. IR (KBr): 3143, 1644, 1495, 1329, 1126 cm⁻¹. ¹H NMR (400 MHz, CDCl₃): δ 3.73 (s, 9H), 3.90 (s, 3H), 6.34 (s, 2H), 6.57 (bs, 1H), 7.38 (d, *J* = 8.8 Hz, 1H), 7.73 (dd, *J* = 2.0, 8.8 Hz, 1H), 7.79 (s, 1H), 8.88 (d, *J* = 2.0 Hz, 1H), 10.00 (s, 1H). ¹³C NMR (100 MHz, CDCl₃): δ 34.0 (CH₃), 56.1 (2) (CH₃), 60.9 (CH₃), 90.1 (2) (CH), 110.3 (CH), 118.7 (C), 122.7 (CH), 123.1 (CH), 124.8 (C), 132.5 (C), 133.3 (C), 135.5 (C), 139.5 (C), 140.7 (CH), 153.5 (2) (C), 184.0 (CH). HRMS (C₁₉H₂₀N₂NaO₆S⁺): calcd. 427.0934 (M + Na⁺), found 427.0935.

3-Formyl-N,1-dimethyl-N-(3,4,5-trimethoxyphenyl)-1H-indole-5-sulfonamide (13). Obtained as described in Method D1 from **12**. Yield: 28%. White solid. IR (KBr): 1660, 1329, 1125, 651 cm⁻¹. ¹H NMR (400 MHz, CDCl₃): δ 3.16 (s, 3H), 3.69 (s, 6H), 3.83 (s, 3H), 3.92 (s, 3H), 6.31 (s, 2H), 7.36 (d, *J* = 8.4 Hz, 1H), 7.50 (dd, *J* = 1.6, 8.4 Hz, 1H), 7.80 (s, 1H), 8.68 (d, *J* = 1.6 Hz, 1H), 10.00 (s, 1H). ¹³C NMR (100 MHz, CDCl₃): δ 34.0 (CH₃), 38.6 (CH₃), 56.2 (2) (CH₃), 60.9 (CH₃), 104.6 (2) (CH), 110.0 (CH), 118.4 (C), 122.6 (CH), 123.4 (CH), 124.4 (C), 131.0 (C), 137.4 (C), 139.4 (C), 140.9 (C), 141.0 (CH), 153.0 (2) (C), 184.0 (CH). HRMS (C₂₀H₂₂N₂NaO₆S⁺): calcd. 441.1091 (M + Na⁺), found 441.1084.

N-Ethyl-3-formyl-1-methyl-N-(3,4,5-trimethoxyphenyl)-1H-indole-5-sulfonamide (14). Obtained as described in Method D1 from **12**. Yield: 11%. Yellow solid. IR (KBr): 1662, 1334, 1124, 653 cm⁻¹. ¹H NMR (400 MHz, CDCl₃): δ 1.09 (t, *J* = 7.2 Hz, 3H), 3.58 (q, *J* = 7.2 Hz, 2H), 3.68 (s, 6H), 3.82 (s, 3H), 3.91 (s, 3H), 6.27 (s, 2H), 7.38 (d, *J* = 8.4 Hz, 1H), 7.60 (dd, *J* = 2.0, 8.4 Hz, 1H), 7.80 (s, 1H), 8.72 (d, *J* = 2.0 Hz, 1H), 10.01 (s, 1H). ¹³C NMR (100 MHz, CDCl₃): δ 13.8 (CH₃), 33.8 (CH₃), 45.7 (CH₂), 55.9 (2) (CH₃), 60.6 (CH₃), 106.3 (2) (CH), 109.6 (CH), 118.4 (C), 122.2 (CH), 123.4 (CH), 124.4 (C), 132.9 (C), 134.4 (C), 137.5 (C), 139.1 (C), 140.3 (CH), 152.8 (2) (C), 183.7 (CH). HRMS (C₂₁H₂₄N₂NaO₆S⁺): calcd. 455.1247 (M + Na⁺), found 455.1210.

3-Cyano-1-methyl-N-(3,4,5-trimethoxyphenyl)-1H-indole-5-sulfonamide (15). Obtained as described in Method G1 from **12**. Yield: 28%. White crystals, m.p. (MeOH/acetone): 236.0–237.4 °C. IR (KBr): 3232, 2231, 1600, 1331, 1126 cm⁻¹. ¹H NMR (400 MHz, CDCl₃): δ 3.73 (s, 6H), 3.76 (s, 3H), 3.93 (s, 3H), 6.32 (s, 2H), 6.56 (bs, 1H), 7.43 (d, *J* = 8.8 Hz, 1H), 7.69 (s, 1H), 7.72 (dd, *J* = 1.6, 8.8 Hz, 1H), 8.32 (d, *J* = 1.6 Hz, 1H). ¹³C NMR (100 MHz, CDCl₃): δ 34.0 (CH₃), 56.2 (2) (CH₃), 60.9 (CH₃), 87.5 (C), 99.4 (2) (CH), 111.0 (CH), 114.3 (C), 120.5 (CH), 122.7 (CH), 127.2 (C), 132.2 (C), 133.0 (C), 135.8 (C), 137.7 (CH), 137.8 (C), 153.5 (2) (C). HRMS (C₁₉H₁₉N₃NaO₅S⁺): calcd. 424.0938 (M + Na⁺), found 424.0940.

3-Cyano-N,1-dimethyl-N-(3,4,5-trimethoxyphenyl)-1H-indole-5-sulfonamide (16). Obtained as described in Method G1 from **13**. Yield: 63%. Light brown crystals, m.p. (CH₂Cl₂/Hex): 182.3–182.8 °C. IR (KBr): 2225, 1595, 1334, 1126, 654 cm⁻¹. ¹H NMR (400 MHz, CDCl₃): δ 3.16 (s, 3H), 3.70 (s, 6H), 3.84 (s, 3H), 3.92 (s, 3H), 6.30 (s, 2H), 7.43 (d, *J* = 8.8 Hz, 1H), 7.52 (dd, *J* = 1.6, 8.8 Hz, 1H), 7.72 (s, 1H), 8.18 (d, *J* = 1.6 Hz, 1H). ¹³C NMR (100 MHz, CDCl₃): δ 34.1 (CH₃), 38.6 (CH₃), 56.2 (2) (CH₃), 60.9 (CH₃), 86.8 (C), 104.6 (2) (CH), 110.8 (CH), 114.5 (C), 120.5 (CH), 123.1 (CH), 126.9 (C), 130.3 (C), 137.2 (C), 137.5 (C), 137.7 (C), 138.2 (CH), 153.0 (2) (C). HRMS (C₂₀H₂₁N₃NaO₅S⁺): calcd. 464.1094 (M + Na⁺), found 464.1097.

(E)-3-(2-Cyanovinyl)-N,1-dimethyl-N-(3,4,5-trimethoxyphenyl)-1H-indole-5-sulfonamide (17E). Obtained as described in Method G2 from **12**. Yield: 33%. Yellow solid. IR (KBr): 2203, 1595, 1334,

1126 cm⁻¹. ¹H NMR (400 MHz, CDCl₃): δ 3.14 (s, 3H), 3.69 (s, 6H), 3.85 (s, 3H), 3.88 (s, 3H), 5.67 (d, *J* = 16.4 Hz, 1H), 6.29 (s, 2H), 7.40 (d, *J* = 8.4 Hz, 1H), 7.46 (s, 1H), 7.47 (d, *J* = 16.4 Hz, 1H), 7.53 (dd, *J* = 1.6, 8.4 Hz, 1H), 8.04 (d, *J* = 1.6 Hz, 1H). ¹³C NMR (100 MHz, CDCl₃): δ 33.3 (CH₃), 38.1 (CH₃), 55.7 (2) (CH₃), 60.5 (CH₃), 91.4 (CH), 104.3 (2) (CH), 109.9 (CH), 112.2 (C), 118.7 (C), 120.5 (CH), 122.2 (CH), 124.2 (C), 129.0 (C), 134.1 (CH), 136.9 (C), 137.1 (C), 139.2 (C), 141.6 (CH), 152.6 (2) (C). HRMS (C₂₂H₂₃N₃NaO₅S⁺): calcd. 464.1251 (M + Na⁺), found 464.1250.

(Z)-3-(2-Cyanovinyl)-N,1-dimethyl-N-(3,4,5-trimethoxyphenyl)-1H-indole-5-sulfonamide (17Z). Obtained as described in Method G2 from **12**. Yield: 9%. Yellow solid. IR (KBr): 2208, 1594, 1335, 1126 cm⁻¹. ¹H NMR (400 MHz, CDCl₃): δ 3.13 (s, 3H), 3.67 (s, 6H), 3.82 (s, 3H), 3.92 (s, 3H), 5.26 (d, *J* = 11.6 Hz, 1H), 6.27 (s, 2H), 7.33 (d, *J* = 11.6 Hz, 1H), 7.41 (d, *J* = 8.8 Hz, 1H), 7.52 (dd, *J* = 1.6, 8.8 Hz, 1H), 7.99 (d, *J* = 1.6 Hz, 1H), 8.31 (s, 1H). ¹³C NMR (100 MHz, CDCl₃): δ 33.7 (CH₃), 38.5 (CH₃), 56.1 (2) (CH₃), 61.0 (CH₃), 89.9 (CH), 104.7 (2) (CH), 110.0 (CH), 111.8 (C), 119.1 (C), 119.6 (CH), 121.0 (CH), 122.4 (C), 126.8 (C), 129.0 (CH), 132.6 (C), 137.4 (C), 138.1 (C), 138.5 (CH), 152.9 (2) (C). HRMS (C₂₂H₂₃N₃NaO₅S⁺): calcd. 464.1239 (M + Na⁺), found 464.1239.

(E)-3-(2-Cyanovinyl)-N-ethyl-1-methyl-N-(3,4,5-trimethoxyphenyl)-1H-indole-5-sulfonamide (18E). Obtained as described in Method G2 from **12**. Yield: 38%. Yellow solid. IR (KBr): 2207, 1619, 1592, 1125, 647 cm⁻¹. ¹H NMR (400 MHz, CDCl₃): δ 1.09 (t, *J* = 7.2 Hz, 3H), 3.53 (q, *J* = 7.2 Hz, 2H), 3.64 (s, 6H), 3.85 (s, 3H), 3.92 (s, 3H), 5.66 (d, *J* = 16.8 Hz, 1H), 6.22 (s, 2H), 7.40 (d, *J* = 8.8 Hz, 1H), 7.44 (d, *J* = 16.8 Hz, 1H), 7.45 (s, 1H), 7.59 (dd, *J* = 1.6, 8.8 Hz, 1H), 8.04 (d, *J* = 1.6 Hz, 1H). ¹³C NMR (100 MHz, CDCl₃): δ 14.1 (CH₃), 33.6 (CH₃), 45.8 (CH₂), 56.1 (2) (CH₃), 61.0 (CH₃), 91.9 (CH), 106.6 (2) (CH), 110.3 (CH), 112.7 (C), 119.0 (C), 120.7 (CH), 122.5 (CH), 124.6 (C), 131.4 (C), 134.4 (CH), 134.5 (C), 137.9 (C), 139.5 (C), 142.0 (CH), 153.1 (2) (C). HRMS (C₂₃H₂₅N₃NaO₅S⁺): calcd. 478.1407 (M + Na⁺), found 478.1405.

(Z)-3-(2-Cyanovinyl)-N-ethyl-1-methyl-N-(3,4,5-trimethoxyphenyl)-1H-indole-5-sulfonamide (18Z). Obtained as described in Method G2 from **12**. Yield: 9%. Yellow solid. IR (KBr): 2204, 1596, 1329, 1125, 652 cm⁻¹. ¹H NMR (400 MHz, CDCl₃): δ 1.09 (t, *J* = 7.2 Hz, 3H), 3.54 (q, *J* = 7.2 Hz, 2H), 3.64 (s, 6H), 3.83 (s, 3H), 3.92 (s, 3H), 5.26 (d, *J* = 12.0 Hz, 1H), 6.21 (s, 2H), 7.34 (d, *J* = 12.0 Hz, 1H), 7.42 (d, *J* = 8.8 Hz, 1H), 7.59 (dd, *J* = 1.6, 8.8 Hz, 1H), 8.01 (d, *J* = 1.6 Hz, 1H), 8.31 (s, 1H). ¹³C NMR (100 MHz, CDCl₃): δ 14.1 (CH₃), 33.9 (CH₃), 45.8 (CH₂), 56.1 (2) (CH₃), 61.0 (CH₃), 89.8 (CH), 106.6 (2) (CH), 110.1 (CH), 111.8 (C), 119.2 (C), 119.4 (CH), 122.3 (CH), 126.8 (C), 130.9 (C), 132.5 (CH), 134.6 (C), 137.8 (C), 138.0 (C), 138.5 (CH), 153.1 (2) (C). HRMS (C₂₃H₂₅N₃NaO₅S⁺): calcd. 478.1407 (M + Na⁺), found 478.1406.

N-(3,5-Dimethoxyphenyl)-1-formylindoline-5-sulfonamide (19). Obtained as described in Method A using 3,5-dimethoxyaniline. Yield: 77%. White solid. IR (KBr): 3202, 2957, 1660, 1584, 1328, 1145, 711 cm⁻¹. ¹H NMR (400 MHz, CDCl₃): δ (E) 3.16 (t, *J* = 8.8 Hz, 2H), 3.72 (s, 6H), 4.10 (t, *J* = 8.8 Hz, 2H), 6.19 (t, *J* = 2.4 Hz, 1H), 6.26 (d, *J* = 2.4 Hz, 2H), 6.73 (bs, 1H), 7.17 (d, *J* = 8.8 Hz, 1H), 7.67 (m, 2H), 8.95 (1H, s). (Z) 3.19 (t, *J* = 8.8 Hz, 2H), 3.72 (s, 6H), 4.18 (t, *J* = 8.8 Hz, 2H), 6.19 (t, *J* = 2.4 Hz, 1H), 6.26 (d, *J* = 2.4 Hz, 2H), 6.73 (bs, 1H), 7.67 (m, 2H), 8.10 (d, *J* = 8.8 Hz, 1H), 8.53 (s, 1H). ¹³C NMR (100 MHz, acetone-d₆): δ 26.4 (CH₂), 27.0 (CH₂), 44.8 (CH₂), 47.0 (CH₂), 55.7 (2) (CH₃), 95.6 (CH), 98.1 (2) (CH), 109.3 (CH), 115.2

(CH), 124.1 (CH), 124.9 (CH), 127.5 (CH), 127.7 (CH), 133.3 (C), 133.9 (C), 134.5 (C), 134.7 (C), 139.7 (C), 139.8 (C), 145.4 (C), 145.7 (C), 158.1 (CH), 160.4 (CH), 161.4 (2) (C).

***N*-(3,5-Dimethoxyphenyl)-1-methylindoline-5-sulfonamide (20).**

Obtained as described in Method B from **19**. Yield: 88%. White powder. IR (KBr): 3241, 2838, 1601, 1306, 1134 cm^{-1} . ^1H NMR (400 MHz, CDCl_3): δ 2.79 (s, 3H), 2.95 (t, $J=8.4$ Hz, 2H), 3.47 (t, $J=8.4$ Hz, 2H), 3.71 (s, 6H), 6.15 (t, $J=2.4$ Hz, 1H), 6.24 (d, $J=2.4$ Hz, 2H), 6.27 (d, $J=8.0$ Hz, 1H), 6.56 (bs, 1H), 7.39 (d, $J=2.0$ Hz, 1H), 7.55 (dd, $J=2.0, 8.0$ Hz, 1H). ^{13}C NMR (100 MHz, CDCl_3): δ 27.7 (CH_2), 34.2 (CH_3), 55.0 (CH_2), 55.4 (2) (CH_3), 96.5 (CH), 98.3 (2) (CH), 104.4 (CH), 123.2 (CH), 125.1 (C), 129.3 (CH), 130.3 (C), 139.2 (C), 156.6 (C), 161.1 (2) (C).

***N*-(3,5-Dimethoxyphenyl)-1-methyl-1H-indole-5-sulfonamide (21).**

Obtained as described in Method C from **20**. Yield: 78%. Brown crystals, m.p. ($\text{CH}_3\text{CN}/\text{MTBE}$): 186–187 °C. IR (KBr): 3241, 2948, 1598, 1312, 1140, 726 cm^{-1} . ^1H NMR (400 MHz, CDCl_3): δ 3.69 (s, 6H), 3.81 (s, 3H), 6.14 (t, $J=2.0$ Hz, 1H), 6.24 (d, $J=2.0$ Hz, 2H), 6.43 (bs, 1H), 6.57 (d, $J=3.2$ Hz, 1H), 7.15 (d, $J=3.2$ Hz, 1H), 7.33 (d, $J=8.4$ Hz, 1H), 7.63 (dd, $J=2.0, 8.4$ Hz, 1H), 8.17 (d, $J=2.0$ Hz, 1H). ^{13}C NMR (100 MHz, CDCl_3): δ 32.8 (CH_3), 55.0 (2) (CH_3), 96.4 (CH), 98.3 (2) (CH), 102.5 (CH), 109.4 (CH), 119.8 (CH), 121.6 (CH), 127.4 (C), 129.1 (C), 130.8 (CH), 138.1 (C), 138.6 (C), 160.7 (2) (C). HRMS ($\text{C}_{17}\text{H}_{18}\text{N}_2\text{NaO}_4\text{S}^+$): calcd. 369.0879 ($\text{M} + \text{Na}^+$), found 369.0878.

***N*-(3,5-Dimethoxyphenyl)-*N*,1-dimethyl-1H-indole-5-sulfonamide (22).**

Obtained as described in Method D1 from **21**. Yield: 91%. White solid. IR (KBr): 2836, 1609, 1330, 1156, 642 cm^{-1} . ^1H NMR (400 MHz, CDCl_3): δ 3.11 (s, 3H), 3.69 (s, 6H), 3.82 (s, 3H), 6.27 (d, $J=2.0$ Hz, 2H), 6.34 (t, $J=2.0$ Hz, 1H), 6.56 (d, $J=3.2$ Hz, 1H), 7.15 (d, $J=3.2$ Hz, 1H), 7.31 (d, $J=8.4$ Hz, 1H), 7.39 (dd, $J=1.6, 8.4$ Hz, 1H), 7.97 (d, $J=1.6$ Hz, 1H). ^{13}C NMR (100 MHz, CDCl_3): δ 33.0 (CH_3), 38.2 (CH_3), 55.3 (2) (CH_3), 99.3 (CH), 102.5 (CH), 104.9 (2) (CH), 109.3 (CH), 120.7 (CH), 122.1 (CH), 126.8 (C), 127.5 (C), 131.3 (CH), 138.4 (C), 143.9 (C), 160.5 (2) (C). HRMS ($\text{C}_{18}\text{H}_{20}\text{N}_2\text{NaO}_4\text{S}^+$): calcd. 383.1036 ($\text{M} + \text{Na}^+$), found 383.1026.

***N*-(3,5-Dimethoxyphenyl)-*N*-ethyl-1-methyl-1H-indole-5-sulfonamide (23).**

Obtained as described in Method D1 from **21**. Yield: 79%. Yellow crystals, m.p. (MeOH): 119–120 °C. IR (KBr): 2968, 1608, 1335, 1159, 643 cm^{-1} . ^1H NMR (400 MHz, CDCl_3): δ 1.06 (t, $J=7.2$ Hz, 3H), 3.54 (q, $J=7.2$ Hz, 2H), 3.68 (s, 6H), 3.84 (s, 3H), 6.21 (d, $J=2.4$ Hz, 2H), 6.38 (t, $J=2.4$ Hz, 1H), 6.57 (d, $J=3.2$ Hz, 1H), 7.16 (d, $J=3.2$ Hz, 1H), 7.33 (d, $J=8.8$ Hz, 1H), 7.48 (dd, $J=2.0, 8.8$ Hz, 1H), 8.01 (d, $J=2.0$ Hz, 1H). ^{13}C NMR (100 MHz, CDCl_3): δ 14.0 (CH_3), 33.1 (CH_3), 45.5 (CH_2), 55.4 (2) (CH_3), 100.2 (CH), 102.7 (CH), 107.2 (2) (CH), 109.1 (CH), 120.8 (CH), 122.1 (CH), 127.6 (C), 129.0 (C), 131.0 (CH), 138.3 (C), 141.2 (C), 160.5 (2) (C). HRMS ($\text{C}_{19}\text{H}_{22}\text{N}_2\text{NaO}_4\text{S}^+$): calcd. 397.1192 ($\text{M} + \text{Na}^+$), found 397.1182.

***Ethyl N*-(3,5-dimethoxyphenyl)-*N*-((1-methyl-1H-indol-5-yl)sulfonyl)-glycinate (24).**

Obtained as described in Method D2 from **21**. Yield: 94%. Yellow crystals, m.p. (MeOH/ CH_2Cl_2): 111–112 °C. IR (KBr): 1748, 1607, 1326, 1150, 640 cm^{-1} . ^1H NMR (400 MHz, CDCl_3): δ 1.21 (t, $J=7.2$ Hz, 3H), 3.65 (s, 6H), 3.83 (s, 3H), 4.14 (q, $J=7.2$ Hz, 2H), 4.36 (s, 2H), 6.33 (t, $J=2.4$ Hz, 1H), 6.35 (d, $J=2.4$ Hz, 2H), 6.56 (d, $J=3.2$ Hz, 1H), 7.15 (d, $J=3.2$ Hz, 1H), 7.33 (d, $J=8.8$ Hz, 1H), 7.55 (dd, $J=2.0, 8.8$ Hz, 1H), 8.06 (d, $J=2.0$ Hz,

1H). ^{13}C NMR (100 MHz, CDCl_3): δ 13.2 (CH_3), 32.2 (CH_3), 51.8 (CH_2), 54.5 (2) (CH_3), 60.5 (CH_2), 99.5 (CH), 101.9 (CH), 105.5 (2) (CH), 108.4 (CH), 120.0 (CH), 121.4 (CH), 126.7 (C), 128.4 (C), 130.2 (CH), 137.6 (C), 141.2 (C), 159.7 (2) (C), 168.0 (C). HRMS ($\text{C}_{21}\text{H}_{24}\text{N}_2\text{NaO}_6\text{S}^+$): calcd. 455.1247 ($\text{M} + \text{Na}^+$), found 455.1246.

***N*-(Cyanomethyl)-*N*-(3,5-dimethoxyphenyl)-1-methyl-1H-indole-5-sulfonamide (25).**

Obtained as described in Method D2 from **21**. Yield: 84%. Brown crystals, m.p. (MeOH/ CH_2Cl_2): 128–129 °C. IR (KBr): 1607, 1342, 1154, 645 cm^{-1} . ^1H NMR (400 MHz, CDCl_3): δ 3.67 (s, 6H), 3.85 (s, 3H), 4.54 (s, 2H), 6.33 (d, $J=2.4$ Hz, 2H), 6.42 (t, $J=2.4$ Hz, 1H), 6.59 (d, $J=3.2$ Hz, 1H), 7.18 (d, $J=3.2$ Hz, 1H), 7.39 (d, $J=8.8$ Hz, 1H), 7.55 (dd, $J=1.6, 8.8$ Hz, 1H), 8.05 (d, $J=1.6$ Hz, 1H). ^{13}C NMR (100 MHz, CDCl_3): δ 33.2 (CH_3), 39.5 (CH_2), 55.4 (2) (CH_3), 101.3 (CH), 102.9 (CH), 106.2 (2) (CH), 109.6 (CH), 115.1 (C), 120.7 (CH), 122.6 (CH), 127.6 (C), 127.8 (C), 131.5 (CH), 138.8 (C), 140.5 (C), 161.0 (2) (C). HRMS ($\text{C}_{19}\text{H}_{19}\text{N}_3\text{NaO}_4\text{S}^+$): calcd. 408.0988 ($\text{M} + \text{Na}^+$), found 408.0977.

***N*-Benzyl-*N*-(3,5-dimethoxyphenyl)-1-methyl-1H-indole-5-sulfonamide (26).**

Obtained as described in Method D2 from **21**. Yield: 82%. Yellow crystals, m.p. (MeOH/ CH_2Cl_2): 124–125 °C. IR (KBr): 1595, 1332, 1152, 642 cm^{-1} . ^1H NMR (400 MHz, CDCl_3): δ 3.59 (s, 6H), 3.86 (s, 3H), 4.67 (s, 2H), 6.14 (d, $J=2.0$ Hz, 2H), 6.27 (t, $J=2.0$ Hz, 1H), 6.59 (d, $J=2.8$ Hz, 1H), 7.18 (d, $J=2.8$ Hz, 1H), 7.21 (m, 5H), 7.37 (d, $J=8.8$ Hz, 1H), 7.53 (dd, $J=1.6, 8.8$ Hz, 1H), 8.07 (d, $J=1.6$ Hz, 1H). ^{13}C NMR (100 MHz, CDCl_3): δ 33.1 (CH_3), 54.7 (CH_2), 55.3 (2) (CH_3), 100.1 (CH), 102.8 (CH), 107.2 (2) (CH), 109.3 (CH), 120.8 (CH), 122.2 (CH), 127.4 (CH), 127.7 (C), 128.3 (2) (CH), 128.5 (2) (CH), 129.2 (C), 131.1 (CH), 136.3 (C), 138.4 (C), 141.3 (C), 160.4 (2) (C). HRMS ($\text{C}_{24}\text{H}_{24}\text{N}_2\text{NaO}_4\text{S}^+$): calcd. 459.1349 ($\text{M} + \text{Na}^+$), found 459.1337.

***N*-(3,5-Dimethoxyphenyl)-*N*-(4-fluorobenzyl)-1-methyl-1H-indole-5-sulfonamide (27).**

Obtained as described in Method D2 from **21**. Yield: 85%. Yellow solid. IR (KBr): 1607, 1150, 1060, 645 cm^{-1} . ^1H NMR (400 MHz, CDCl_3): δ 3.60 (s, 6H), 3.84 (s, 3H), 4.63 (s, 2H), 6.12 (d, $J=2.4$ Hz, 2H), 6.29 (t, $J=2.4$ Hz, 1H), 6.59 (d, $J=3.2$ Hz, 1H), 6.90 (t, $J=8.4$ Hz, 2H), 7.20 (d, $J=3.2$ Hz, 1H), 7.22 (dd, $J=5.2, 8.4$ Hz, 2H), 7.36 (d, $J=8.8$ Hz, 1H), 7.51 (dd, $J=1.6, 8.8$ Hz, 1H), 8.06 (d, $J=1.6$ Hz, 1H). ^{13}C NMR (100 MHz, CDCl_3): δ 33.1 (CH_3), 54.0 (CH_2), 55.3 (2) (CH_3), 100.1 (CH), 102.7 (CH), 107.2 (2) (CH), 109.4 (CH), 115.2 (2) (d, $J=21.4$ Hz, CH), 120.7 (CH), 122.1 (CH), 127.7 (C), 129.0 (C), 130.2 (2) (d, $J=8.0$ Hz, CH), 131.2 (CH), 132.1 (C), 138.4 (C), 141.1 (C), 160.4 (2) (C), 162.2 (d, $J=244.4$ Hz, C). HRMS ($\text{C}_{24}\text{H}_{24}\text{FN}_2\text{O}_4\text{S}^+$): calcd. 455.1435 ($\text{M} + \text{H}^+$), found 455.1418.

5-(*N*-(3,5-Dimethoxyphenyl)sulfamoyl)-1-methyl-1H-indole-3-carboxamide (28).

CSI (47 μL , 0.53 mmol) was added dropwise to **21** (123 mg, 0.36 mmol) in 1,2-dichloroethane (15 mL) at 4 °C, and warmed to room temperature under N_2 . After 24 h, the reaction mixture was rotary evaporated. Crystallisation from methanol yielded **28** (80 mg, 0.21 mmol, 58%). Red crystals, m.p. (MeOH): 229–231 °C. IR (KBr): 3381, 1641, 1609, 1322, 1145, 657 cm^{-1} . ^1H NMR (400 MHz, $\text{DMSO}-d_6$): δ 3.58 (s, 6H), 3.80 (s, 3H), 6.04 (bs, 1H), 6.25 (bs, 2H), 7.59 (m, 2H), 8.09 (s, 1H), 8.71 (bs, 1H), 10.20 (bs, 1H). ^{13}C NMR (100 MHz, $\text{DMSO}-d_6$): δ 33.7 (CH_3), 55.5 (2) (CH_3), 95.3 (CH), 97.6 (2) (CH), 111.0 (C), 111.5 (CH), 120.6 (CH), 122.1 (CH), 126.4 (C), 132.0 (C), 134.8 (CH), 138.7 (C), 140.4 (C), 161.0 (2) (C), 165.9 (C). HRMS ($\text{C}_{18}\text{H}_{19}\text{N}_3\text{NaO}_5\text{S}^+$): calcd. 412.0938 ($\text{M} + \text{Na}^+$), found 412.0943.

***N*-(3,5-Dimethoxyphenyl)-3-formyl-*N*,1-dimethyl-1*H*-indole-5-sulfonamide (29).** Obtained as described in Method F from **22**. Yield: 82%. Yellow crystals, m.p. (methanol/CH₂Cl₂): 194–195 °C. IR (KBr): 1663, 1610, 1333, 1157, 634 cm⁻¹. ¹H NMR (400 MHz, CDCl₃): δ 3.16 (s, 3H), 3.71 (s, 6H), 3.92 (s, 3H), 6.27 (d, *J* = 2.0 Hz, 2H), 6.35 (t, *J* = 2.0 Hz, 1H), 7.35 (d, *J* = 8.4 Hz, 1H), 7.46 (dd, *J* = 2.0, 8.4 Hz, 1H), 7.79 (s, 1H), 8.67 (d, *J* = 2.0 Hz, 1H), 10.00 (s, 1H). ¹³C NMR (100 MHz, CDCl₃): δ 34.0 (CH₃), 38.3 (CH₃), 55.4 (2) (CH₃), 99.4 (CH), 104.9 (2) (CH), 110.0 (CH), 118.5 (C), 122.6 (CH), 123.3 (CH), 124.5 (C), 131.0 (C), 139.5 (C), 140.5 (CH), 143.5 (C), 160.6 (2) (C), 184.0 (CH). HRMS (C₁₉H₂₀N₂NaO₅S⁺): calcd. 411.0985 (M + Na⁺), found 411.0977.

***N*-Benzyl-*N*-(3,5-dimethoxyphenyl)-3-formyl-1-methyl-1*H*-indole-5-sulfonamide (30).** Obtained as described in Method F from **26**. Yield: 97%. Yellow crystals, m.p. (MeOH/CH₂Cl₂): 162–163 °C. IR (KBr): 1662, 1605, 1330, 1163, 697 cm⁻¹. ¹H NMR (400 MHz, CDCl₃): δ 3.61 (s, 6H), 3.94 (s, 3H), 4.72 (s, 2H), 6.14 (d, *J* = 2.4 Hz, 2H), 6.27 (t, *J* = 2.4 Hz, 1H), 7.22 (m, 5H), 7.40 (d, *J* = 8.8 Hz, 1H), 7.61 (dd, *J* = 2.0, 8.8 Hz, 1H), 7.82 (s, 1H), 8.77 (d, *J* = 2.0 Hz, 1H), 10.02 (s, 1H). ¹³C NMR (100 MHz, CDCl₃): δ 34.0 (CH₃), 54.9 (CH₂), 55.3 (2) (CH₃), 100.1 (CH), 107.2 (2) (CH), 110.1 (CH), 118.7 (C), 122.4 (CH), 123.4 (CH), 124.8 (C), 127.5 (CH), 128.3 (2) (CH), 128.5 (2) (CH), 133.3 (C), 136.1 (C), 139.5 (C), 140.3 (CH), 140.9 (C), 160.4 (2) (C), 183.9 (CH). HRMS (C₂₅H₂₄N₂NaO₅S⁺): calcd. 487.1298 (M + Na⁺), found 487.1297.

3-Cyano-*N*-(3,5-dimethoxyphenyl)-*N*,1-dimethyl-1*H*-indole-5-sulfonamide (31). Obtained as described in Method G1 from **29**. Yield: 24%. Brown crystals, m.p. (MeOH/CH₂Cl₂): 163–164 °C. IR (KBr): 2221, 1607, 1335, 1204, 657 cm⁻¹. ¹H NMR (400 MHz, CDCl₃): δ 3.14 (s, 3H), 3.72 (s, 6H), 3.90 (s, 3H), 6.24 (d, *J* = 2.4 Hz, 2H), 6.36 (t, *J* = 2.4 Hz, 1H), 7.40 (d, *J* = 8.8 Hz, 1H), 7.47 (dd, *J* = 1.6, 8.8 Hz, 1H), 7.69 (s, 1H), 8.10 (d, *J* = 1.6 Hz, 1H). ¹³C NMR (100 MHz, CDCl₃): δ 34.0 (CH₃), 38.3 (CH₃), 55.5 (2) (CH₃), 87.3 (C), 99.4 (CH), 105.0 (2) (CH), 110.7 (CH), 114.5 (C), 120.6 (CH), 123.1 (CH), 126.9 (C), 130.5 (C), 137.7 (C), 137.8 (CH), 143.3 (C), 160.6 (2) (C). HRMS (C₁₉H₁₉N₃NaO₄S⁺): calcd. 408.0988 (M + Na⁺), found 408.0984.

***N*-Benzyl-3-cyano-*N*-(3,5-dimethoxyphenyl)-1-methyl-1*H*-indole-5-sulfonamide (32).** Obtained as described in Method G1 from **30**. Yield: 27%. Brown crystals, m.p. (CH₂Cl₂/Hex): 191–193 °C. IR (KBr): 2223, 1601, 1165, 656 cm⁻¹. ¹H NMR (400 MHz, CDCl₃): δ 3.63 (s, 6H), 3.93 (s, 3H), 4.71 (s, 2H), 6.12 (d, *J* = 2.4 Hz, 2H), 6.30 (t, *J* = 2.4 Hz, 1H), 7.25 (m, 5H), 7.46 (d, *J* = 8.8 Hz, 1H), 7.64 (dd, *J* = 1.6, 8.8 Hz, 1H), 7.71 (s, 1H), 8.21 (d, *J* = 1.6 Hz, 1H). ¹³C NMR (100 MHz, CDCl₃): δ 34.0 (CH₃), 54.9 (CH₂), 55.3 (2) (CH₃), 87.4 (C), 100.0 (CH), 107.2 (2) (CH), 110.8 (CH), 114.5 (C), 120.5 (CH), 123.1 (CH), 127.0 (C), 127.7 (CH), 128.3 (2) (CH), 128.5 (2) (CH), 132.7 (C), 135.9 (C), 137.6 (C), 137.7 (CH), 140.8 (C), 160.5 (2) (C). HRMS (C₂₅H₂₃N₃NaO₄S⁺): calcd. 484.1301 (M + Na⁺), found 484.1286.

***N*-(2,5-Dimethoxyphenyl)-1-formylindoline-5-sulfonamide (33).** Obtained as described in Method A using 2,5-dimethoxyaniline. Yield: 79%. White powder. IR (KBr): 3228, 1672, 1496, 1325 cm⁻¹. ¹H NMR (400 MHz, CDCl₃): δ (E) 3.14 (t, *J* = 8.4 Hz, 2H), 3.66 (s, 3H), 3.75 (s, 3H), 4.08 (t, *J* = 8.4 Hz, 2H), 6.55 (dd, *J* = 3.2, 8.8 Hz, 1H), 6.68 (d, *J* = 8.8 Hz, 1H), 7.04 (bs, 1H), 7.13 (m, 2H), 7.65 (m, 2H), 8.93 (s, 1H). (Z) 3.19 (t, *J* = 8.8 Hz, 2H), 3.65 (s, 3H), 3.74 (s, 3H), 4.16 (t, *J* = 8.8 Hz, 2H), 6.53 (dd, *J* = 3.2, 8.8 Hz, 1H), 6.66 (d, *J* = 8.8 Hz, 1H), 7.04 (bs, 1H), 7.13 (m, 1H), 7.65 (m, 2H), 8.07 (d, *J* = 8.0 Hz, 1H), 8.51 (s, 1H). ¹³C NMR (100 MHz, CDCl₃): δ 26.7

(CH₂), 27.2 (CH₂), 45.2 (CH₂), 47.2 (CH₂), 55.8 (CH₃), 56.2 (CH₃), 106.9 (CH), 108.9 (CH), 109.5 (CH), 111.4 (CH), 116.1 (CH), 124.1 (CH), 125.3 (CH), 126.6 (C), 128.0 (CH), 132.8 (C), 134.5 (C), 143.4 (C), 145.2 (C), 153.9 (C), 157.6 (CH), 159.8 (CH). GC-MS (C₁₇H₁₈N₂O₂S⁺): 362 (M⁺).

***N*-(2,5-Dimethoxyphenyl)-1-methylindoline-5-sulfonamide (34).** Obtained as described in Method B from **33**. Yield: 91%. White powder. IR (KBr): 3283, 1602, 1513, 1322 cm⁻¹. ¹H NMR (400 MHz, CDCl₃): δ 2.78 (s, 3H), 2.93 (t, *J* = 8.4 Hz, 2H), 3.44 (t, *J* = 8.4 Hz, 2H), 3.66 (s, 3H), 3.73 (s, 3H), 6.25 (d, *J* = 8.8 Hz, 1H), 6.49 (dd, *J* = 2.8, 8.8 Hz, 1H), 6.66 (d, *J* = 8.8 Hz, 1H), 7.01 (bs, 1H), 7.11 (d, *J* = 2.8 Hz, 1H), 7.39 (d, *J* = 2.0 Hz, 1H), 7.54 (dd, *J* = 2.0, 8.8 Hz, 1H). ¹³C NMR (100 MHz, CDCl₃): δ 25.5 (CH₂), 32.1 (CH₃), 52.8 (CH₂), 53.6 (CH₃), 54.3 (CH₃), 102.2 (CH), 104.0 (CH), 106.6 (CH), 109.3 (CH), 121.0 (CH), 123.3 (C), 125.5 (C), 127.0 (CH), 128.0 (C), 141.0 (C), 151.8 (C), 154.5 (C). GC-MS (C₁₇H₂₀N₂O₄S⁺): 348 (M⁺).

***N*-(2,5-Dimethoxyphenyl)-1-methyl-1*H*-indole-5-sulfonamide (35).** Obtained as described in Method C from **34**. Yield: 72%. Purple crystals, m.p. (CH₃CN/MTBE): 153.8–154.8 °C. IR (KBr): 3258, 1510, 1122, 636 cm⁻¹. ¹H NMR (400 MHz, CDCl₃): δ 3.58 (s, 3H), 3.72 (s, 3H), 3.78 (s, 3H), 6.46 (dd, *J* = 2.8, 8.8 Hz, 1H), 6.55 (d, 3.2 Hz, 1H), 6.60 (d, *J* = 8.8 Hz, 1H), 7.12 (bs, 1H), 7.13 (d, *J* = 2.8 Hz, 1H), 7.18 (d, *J* = 3.2 Hz, 1H), 7.29 (d, *J* = 8.8 Hz, 1H), 7.63 (dd, *J* = 1.6, 8.8 Hz, 1H), 8.16 (d, *J* = 1.6 Hz, 1H). ¹³C NMR (100 MHz, CDCl₃): δ 33.0 (CH₃), 55.7 (CH₃), 56.3 (CH₃), 102.7 (CH), 106.3 (CH), 109.0 (CH), 109.4 (CH), 111.5 (CH), 120.1 (CH), 121.8 (CH), 127.3 (C), 127.6 (C), 129.7 (C), 131.1 (CH), 138.4 (C), 143.2 (C), 153.9 (C). HRMS (C₁₇H₁₈N₂NaO₄S⁺): calcd. 369.0879 (M + Na⁺), found 369.0868.

***N*-(2,5-Dimethoxyphenyl)-*N*,1-dimethyl-1*H*-indole-5-sulfonamide (36).** Obtained as described in Method D1 from **35**. Yield: 94%. Yellow solid. IR (KBr): 1505, 1328, 1216, 640 cm⁻¹. ¹H NMR (400 MHz, CDCl₃): δ 3.18 (s, 3H), 3.32 (s, 3H), 3.71 (s, 3H), 3.83 (s, 3H), 6.56 (d, *J* = 3.6 Hz, 1H), 6.71 (d, *J* = 8.4 Hz, 1H), 6.81 (dd, *J* = 2.8, 8.4 Hz, 1H), 6.83 (d, *J* = 2.8 Hz, 1H), 7.15 (d, *J* = 3.6 Hz, 1H), 7.34 (d, *J* = 8.4 Hz, 1H), 7.57 (dd, *J* = 1.6, 8.4 Hz, 1H), 8.05 (d, *J* = 1.6 Hz, 1H). ¹³C NMR (100 MHz, CDCl₃): δ 33.1 (CH₃), 37.9 (CH₃), 55.6 (CH₃), 55.8 (CH₃), 102.5 (CH), 108.9 (CH), 112.6 (CH), 114.6 (CH), 116.7 (CH), 120.9 (CH), 121.9 (CH), 127.6 (C), 129.9 (C), 130.2 (C), 130.8 (CH), 138.2 (C), 150.9 (C), 153.1 (C). HRMS (C₁₈H₂₀N₂NaO₄S⁺): calcd. 383.1036 (M + Na⁺), found 383.1039.

Ethyl *N*-(2,5-dimethoxyphenyl)-*N*-((1-methyl-1*H*-indol-5-yl)sulfonyl)-glycinate (37). Obtained as described in Method D2 from **35**. Yield: 60%. Orange crystals, m.p. (MeOH): 116–117 °C. IR (KBr): 1749, 1503, 1336, 644 cm⁻¹. ¹H NMR (400 MHz, CDCl₃): δ 1.22 (d, *J* = 7.2 Hz, 3H), 3.22 (s, 3H), 3.71 (s, 3H), 3.82 (s, 3H), 4.13 (q, *J* = 7.2 Hz, 2H), 4.42 (s, 2H), 6.54 (d, *J* = 3.2 Hz, 1H), 6.64 (d, *J* = 8.8 Hz, 1H), 6.80 (dd, *J* = 3.2, 8.8 Hz, 1H), 7.12 (d, *J* = 3.2 Hz, 1H), 7.13 (d, *J* = 3.2 Hz, 1H), 7.31 (d, *J* = 8.4 Hz, 1H), 7.55 (dd, *J* = 2.0, 8.4 Hz, 1H), 8.00 (d, *J* = 2.0 Hz, 1H). ¹³C NMR (100 MHz, CDCl₃): δ 14.1 (CH₃), 33.1 (CH₃), 51.2 (CH₂), 55.4 (CH₃), 55.7 (CH₃), 61.1 (CH₂), 102.6 (CH), 108.8 (CH), 112.1 (CH), 115.4 (CH), 118.7 (CH), 120.7 (CH), 121.8 (CH), 127.5 (C), 127.7 (C), 130.8 (CH), 130.9 (C), 138.3 (C), 150.2 (C), 153.0 (C), 169.6 (C). HRMS (C₂₁H₂₄N₂NaO₆S⁺): calcd. 455.1247 (M + Na⁺), found 455.1232.

***N*-(Cyanomethyl)-*N*-(2,5-dimethoxyphenyl)-1-methyl-1*H*-indole-5-sulfonamide (38).** Obtained as described in Method D2 from **35**. Yield: 47%. Yellow crystals, m.p. (CH₂Cl₂/Hex): 150.0–150.4 °C. IR

(KBr): 1502, 1325, 1145 cm^{-1} . ^1H NMR (400 MHz, CDCl_3): δ 3.29 (s, 3H), 3.70 (s, 3H), 3.84 (s, 3H), 4.59 (s, 2H), 6.57 (d, $J=3.2$ Hz, 1H), 6.71 (d, $J=9.2$ Hz, 1H), 6.87 (dd, $J=3.2, 9.2$ Hz, 1H), 6.91 (d, $J=3.2$ Hz, 1H), 7.17 (d, $J=3.2$ Hz, 1H), 7.36 (d, $J=9.2$ Hz, 1H), 7.56 (dd, $J=2.0, 9.2$ Hz, 1H), 8.01 (d, $J=2.0$ Hz, 1H). ^{13}C NMR (100 MHz, CDCl_3): δ 33.2 (CH_3), 38.4 (CH_2), 55.5 (CH_3), 55.8 (CH_3), 102.8 (CH), 109.3 (CH), 112.6 (CH), 115.6 (C), 116.3 (CH), 117.4 (CH), 120.6 (CH), 122.1 (CH), 126.2 (C), 127.7 (C), 129.3 (C), 131.2 (CH), 138.6 (C), 150.3 (C), 153.4 (C). HRMS ($\text{C}_{19}\text{H}_{20}\text{N}_3\text{O}_4\text{S}^+$): calcd. 386.1169 ($\text{M} + \text{H}^+$), found 386.1170.

***N*-Benzyl-*N*-(2,5-dimethoxyphenyl)-1-methyl-1*H*-indole-5-sulfonamide (39).** Obtained as described in Method D2 from **35**. Yield: 62%. White solid. IR (KBr): 1503, 1333, 1149, 642 cm^{-1} . ^1H NMR (400 MHz, CDCl_3): δ 3.20 (s, 3H), 3.60 (s, 3H), 3.83 (s, 3H), 4.76 (s, 2H), 6.55 (d, $J=3.2$ Hz, 1H), 6.61 (d, $J=8.8$ Hz, 1H), 6.64 (d, $J=3.2$ Hz, 1H), 6.72 (dd, $J=3.2, 8.8$ Hz, 1H), 7.15 (d, $J=3.2$ Hz, 1H), 7.21 (m, 5H), 7.34 (d, $J=8.8$ Hz, 1H), 7.61 (dd, $J=1.6, 8.8$ Hz, 1H), 8.06 (d, $J=1.6$ Hz, 1H). ^{13}C NMR (100 MHz, CDCl_3): δ 33.1 (CH_3), 53.6 (CH_2), 55.4 (CH_3), 55.7 (CH_3), 102.5 (CH), 109.0 (CH), 112.2 (CH), 114.7 (CH), 118.9 (CH), 120.8 (CH), 121.8 (CH), 127.3 (CH), 127.5 (C), 127.6 (C), 128.1 (2) (CH), 128.7 (2) (CH), 131.0 (CH), 137.1 (C), 138.3 (C), 151.1 (C), 152.9 (C). Quaternary carbon not observed. HRMS ($\text{C}_{24}\text{H}_{24}\text{N}_3\text{NaO}_4\text{S}^+$): calcd. 459.1349 ($\text{M} + \text{Na}^+$), found 459.1339.

***N*-(2,5-Dimethoxyphenyl)-3-formyl-1-methyl-1*H*-indole-5-sulfonamide (40).** Obtained as described in Method F from **35**. Yield: 96%. Brown solid. IR (KBr): 3104, 1644, 1509, 1168 cm^{-1} . ^1H NMR (400 MHz, CDCl_3): δ 3.64 (s, 3H), 3.75 (s, 3H), 3.87 (s, 3H), 6.47 (dd, $J=3.2, 8.8$ Hz, 1H), 6.61 (d, $J=8.8$ Hz, 1H), 7.19 (d, $J=3.2$ Hz, 1H), 7.20 (bs, 1H), 7.34 (d, $J=8.4$ Hz, 1H), 7.73 (s, 1H), 7.79 (dd, $J=1.6, 8.4$ Hz, 1H), 8.84 (d, $J=1.6$ Hz, 1H), 9.97 (s, 1H). ^{13}C NMR (100 MHz, acetone- d_6): δ 33.2 (CH_3), 54.9 (CH_3), 55.8 (CH_3), 107.2 (CH), 109.0 (CH), 110.9 (CH), 112.0 (CH), 118.3 (C), 121.8 (CH), 122.2 (CH), 124.3 (C), 127.4 (C), 134.0 (C), 139.8 (C), 142.6 (CH), 144.1 (C), 153.8 (C), 184.0 (CH). HRMS ($\text{C}_{18}\text{H}_{18}\text{N}_2\text{NaO}_5\text{S}^+$): calcd. 397.0829 ($\text{M} + \text{Na}^+$), found 397.0827.

***N*-(2,5-Dimethoxyphenyl)-3-formyl-*N*,1-dimethyl-1*H*-indole-5-sulfonamide (41).** Obtained as described in Method D1 from **40**. Yield: 89%. Yellow crystals, m.p. ($\text{CH}_2\text{Cl}_2/\text{Hex}$): 169.2–170.3 $^\circ\text{C}$. IR (KBr): 1661, 1508, 1329, 1041 cm^{-1} . ^1H NMR (400 MHz, CDCl_3): δ 3.19 (s, 3H), 3.66 (s, 3H), 3.74 (s, 3H), 3.92 (s, 3H), 6.72 (d, $J=8.8$ Hz, 1H), 6.82 (dd, $J=2.8, 8.8$ Hz, 1H), 6.87 (d, $J=2.8$ Hz, 1H), 7.37 (d, $J=8.8$ Hz, 1H), 7.71 (dd, $J=2.0, 8.8$ Hz, 1H), 7.72 (s, 1H), 8.74 (d, $J=2.0$ Hz, 1H), 10.01 (s, 1H). ^{13}C NMR (100 MHz, CDCl_3): δ 33.9 (CH_3), 37.8 (CH_3), 55.4 (CH_3), 55.8 (CH_3), 109.7 (CH), 112.5 (CH), 114.6 (CH), 116.9 (CH), 118.3 (C), 122.2 (CH), 123.3 (CH), 124.3 (C), 129.8 (C), 133.7 (C), 139.3 (C), 140.9 (CH), 150.7 (C), 153.2 (C), 184.1 (CH). HRMS ($\text{C}_{19}\text{H}_{20}\text{N}_2\text{NaO}_5\text{S}^+$): calcd. 411.0985 ($\text{M} + \text{Na}^+$), found 411.0982.

3-Cyano-*N*-(2,5-dimethoxyphenyl)-1-methyl-1*H*-indole-5-sulfonamide (42). Obtained as described in Method G1 from **40**. Yield: 28%. White solid. IR (KBr): 3217, 3108, 2220, 1510, 1331, 1159, 688 cm^{-1} . ^1H NMR (400 MHz, CDCl_3): δ 3.64 (s, 3H), 3.74 (s, 3H), 3.86 (s, 3H), 6.50 (dd, $J=2.8, 9.2$ Hz, 1H), 6.62 (d, $J=9.2$ Hz, 1H), 7.16 (bs, 1H), 7.17 (d, $J=2.8$ Hz, 1H), 7.39 (d, $J=8.8$ Hz, 1H), 7.64 (s, 1H), 7.77 (dd, $J=1.6, 8.8$ Hz, 1H), 8.29 (d, $J=1.6$ Hz, 1H). ^{13}C NMR (100 MHz, CDCl_3): δ 34.0 (CH_3), 55.8 (CH_3), 56.2 (CH_3), 87.5 (C), 106.6 (CH), 109.7 (CH), 110.8 (CH), 111.4 (CH), 114.3 (C), 120.3

(CH), 122.6 (CH), 126.6 (C), 127.0 (C), 133.2 (C), 137.6 (CH), 137.7 (C), 143.2 (C), 153.9 (C). HRMS ($\text{C}_{18}\text{H}_{17}\text{N}_3\text{NaO}_4\text{S}^+$): calcd. 394.0832 ($\text{M} + \text{Na}^+$), found 394.0837.

***N*-((3-Cyano-1-methyl-1*H*-indol-5-yl)sulfonyl)-*N*-(2,5-dimethoxyphenyl)acetamide (43).** Obtained as byproduct in the preparation of **42**. Yield: 27%. White solid. IR (KBr): 2219, 1703, 1508, 1356, 1148 cm^{-1} . ^1H NMR (400 MHz, CDCl_3): δ 1.82 (s, 3H), 3.83 (s, 3H), 3.84 (s, 3H), 3.92 (s, 3H), 7.01 (m, 3H), 7.52 (d, $J=9.2$ Hz, 1H), 7.71 (s, 1H), 8.22 (dd, $J=1.6, 9.2$ Hz, 1H), 8.51 (d, $J=1.6$ Hz, 1H). ^{13}C NMR (100 MHz, CDCl_3): δ 23.9 (CH_3), 34.0 (CH_3), 55.7 (CH_3), 55.9 (CH_3), 87.6 (C), 109.9 (CH), 112.6 (CH), 114.5 (C), 117.0 (CH), 117.4 (CH), 122.1 (CH), 125.3 (C), 125.7 (CH), 126.9 (C), 133.7 (C), 137.6 (CH), 138.3 (C), 150.0 (C), 153.7 (C), 170.4 (C). HRMS ($\text{C}_{20}\text{H}_{19}\text{N}_3\text{NaO}_5\text{S}^+$): calcd. 436.0938 ($\text{M} + \text{Na}^+$), found 436.0943.

(*E*)-3-(2-Cyanovinyl)-*N*-(2,5-dimethoxyphenyl)-1-methyl-1*H*-indole-5-sulfonamide (44E). Obtained as described in Method G2 from **40**. Yield: 20%. White solid. IR (KBr): 3242, 2210, 1618, 1509, 1169, 644 cm^{-1} . ^1H NMR (400 MHz, CDCl_3): δ 3.52 (s, 3H), 3.69 (s, 3H), 3.76 (s, 3H), 5.60 (d, $J=16.4$ Hz, 1H), 6.45 (dd, $J=3.2, 8.8$ Hz, 1H), 6.56 (d, $J=8.8$ Hz, 1H), 7.06 (bs, 1H), 7.17 (d, $J=3.2$ Hz, 1H), 7.29 (d, $J=8.8$ Hz, 1H), 7.32 (s, 1H), 7.41 (d, $J=16.4$ Hz, 1H), 7.70 (dd, $J=1.6, 8.8$ Hz, 1H), 8.11 (d, $J=1.6$ Hz, 1H). ^{13}C NMR (100 MHz, CDCl_3): δ 33.5 (CH_3), 55.7 (CH_3), 56.2 (CH_3), 91.9 (CH), 107.1 (CH), 109.3 (CH), 110.5 (CH), 111.4 (CH), 112.8 (C), 119.2 (C), 120.2 (CH), 121.9 (CH), 124.6 (C), 126.9 (C), 132.3 (CH), 134.4 (C), 139.7 (CH), 142.0 (C), 143.4 (C), 153.9 (C). HRMS ($\text{C}_{20}\text{H}_{19}\text{N}_3\text{NaO}_4\text{S}^+$): calcd. 420.0988 ($\text{M} + \text{H}^+$), found 420.0997.

(*Z*)-3-(2-Cyanovinyl)-*N*-(2,5-dimethoxyphenyl)-1-methyl-1*H*-indole-5-sulfonamide (44Z). Obtained as described in Method G2 from **40**. Yield: 10%. Yellow solid. IR (KBr): 3249, 2207, 1508, 1167, 646 cm^{-1} . ^1H NMR (400 MHz, CDCl_3): δ 3.57 (s, 3H), 3.73 (s, 3H), 3.88 (s, 3H), 5.27 (d, $J=12.0$ Hz, 1H), 6.50 (dd, $J=2.8, 9.2$ Hz, 1H), 6.61 (d, $J=9.2$ Hz, 1H), 7.11 (bs, NH), 7.17 (d, $J=2.8$ Hz, 1H), 7.35 (d, $J=12.0$ Hz, 1H), 7.36 (d, $J=8.8$ Hz, 1H), 7.70 (dd, $J=1.6, 8.8$ Hz, H6), 8.19 (d, $J=1.6$ Hz, 1H), 8.28 (s, 1H). ^{13}C NMR (100 MHz, CDCl_3): δ 31.6 (CH_3), 53.6 (CH_3), 54.0 (CH_3), 87.4 (CH), 104.7 (CH), 107.2 (CH), 108.1 (CH), 109.2 (CH), 109.7 (C), 116.7 (CH), 117.0 (C), 119.3 (CH), 124.7 (C), 129.6 (C), 130.4 (CH), 136.0 (CH), 136.4 (C), 141.2 (C), 151.7 (C). Quaternary carbon not observed. HRMS ($\text{C}_{20}\text{H}_{19}\text{N}_3\text{NaO}_4\text{S}^+$): calcd. 420.0988 ($\text{M} + \text{H}^+$), found 420.0985.

3-Bromo-*N*-(4-bromo-2,5-dimethoxyphenyl)-1-methyl-1*H*-indole-5-sulfonamide (45). Obtained as described in Method E from **35**. Yield: 50%. White crystals, m.p. ($\text{MeOH}/\text{CH}_2\text{Cl}_2$): 174.5–175.1 $^\circ\text{C}$. IR (KBr): 3269, 1501, 1326, 1139, 672 cm^{-1} . ^1H NMR (400 MHz, CDCl_3): δ 3.69 (s, 3H), 3.79 (s, 3H), 3.86 (s, 3H), 6.86 (s, 1H), 7.10 (bs, 1H), 7.18 (s, 1H), 7.25 (s, 1H), 7.30 (d, $J=8.4$ Hz, 1H), 7.62 (dd, $J=1.6, 8.4$ Hz, 1H), 8.12 (d, $J=1.6$ Hz, 1H). ^{13}C NMR (100 MHz, CDCl_3): δ 33.1 (CH_3), 56.2 (CH_3), 56.6 (CH_3), 90.7 (C), 104.7 (CH), 105.3 (C), 109.8 (CH), 115.5 (CH), 120.3 (CH), 120.7 (CH), 125.9 (C), 126.4 (C), 129.8 (CH), 129.9 (C), 137.8 (C), 143.0 (C), 149.9 (C). HRMS ($\text{C}_{17}\text{H}_{16}\text{Br}_2\text{N}_2\text{NaO}_4\text{S}^+$): calcd. 524.9090 ($\text{M} + \text{Na}^+$), found 524.9099.

3-Bromo-*N*-(4-bromo-2,5-dimethoxyphenyl)-*N*,1-dimethyl-1*H*-indole-5-sulfonamide (46). Obtained as described in Method D1 from **45**. Yield: 49%. Yellow crystals, m.p. ($\text{MeOH}/\text{CH}_2\text{Cl}_2$): 124.0–125.2 $^\circ\text{C}$. IR (KBr): 1495, 1338, 1217, 697 cm^{-1} . ^1H NMR (400 MHz, CDCl_3): δ 3.17 (s, 3H), 3.30 (s, 3H), 3.82 (s, 3H), 3.83 (s, 3H), 6.92 (s, 1H), 6.98 (s, 1H), 7.20 (s, 1H), 7.34 (d, $J=8.8$ Hz, 1H),

7.60 (dd, $J=1.6, 8.8$ Hz, 1H), 8.00 (d, $J=1.6, 1$ H). ^{13}C NMR (100 MHz, CDCl_3): δ 33.4 (CH_3), 37.7 (CH_3), 55.7 (CH_3), 56.9 (CH_3), 90.8 (C), 109.4 (CH), 111.4 (C), 115.6 (CH), 116.8 (CH), 120.4 (CH), 121.9 (CH), 126.7 (C), 129.0 (C), 129.9 (CH), 130.9 (C), 137.9 (C), 149.7 (C), 150.7 (C). HRMS ($\text{C}_{18}\text{H}_{18}\text{Br}_2\text{N}_2\text{NaO}_4\text{S}^+$): calcd. 538.9246 ($\text{M} + \text{Na}^+$), found 538.9249.

***N*-(4-Bromo-2,5-dimethoxyphenyl)-3-formyl-1-methyl-1H-indole-5-sulfonamide (47)**. Obtained as described in Method E from **40**. Yield: 68%. Light brown crystals, m.p. (MeOH/acetone): 224.0–224.7 °C. IR (KBr): 3105, 1648, 1330, 1169, 723 cm^{-1} . ^1H NMR (400 MHz, CDCl_3): δ 3.61 (s, 3H), 3.84 (s, 3H), 3.86 (s, 3H), 6.82 (s, 1H), 7.13 (bs, 1H), 7.24 (s, 1H), 7.33 (d, $J=8.4$ Hz, 1H), 7.72 (dd, $J=2.0, 8.4$ Hz, 1H), 7.74 (s, 1H), 8.84 (d, $J=2.0$ Hz, 1H), 9.96 (s, 1H). ^{13}C NMR (100 MHz, CDCl_3): δ 34.0 (CH_3), 56.4 (CH_3), 56.9 (CH_3), 104.7 (CH), 105.5 (C), 110.3 (CH), 115.7 (CH), 118.7 (C), 122.7 (CH), 122.8 (CH), 124.6 (C), 126.2 (C), 133.1 (C), 139.6 (C), 140.6 (CH), 143.1 (C), 150.3 (C), 183.9 (CH). HRMS ($\text{C}_{18}\text{H}_{17}\text{BrN}_2\text{NaO}_5\text{S}^+$): calcd. 474.9934 ($\text{M} + \text{Na}^+$), found 474.9936.

***N*-(4-Bromo-2,5-dimethoxyphenyl)-3-formyl-N,1-dimethyl-1H-indole-5-sulfonamide (48)**. Obtained as described in Method E from **41**. Yield: 35%. Yellow crystals, m.p. ($\text{CH}_2\text{Cl}_2/\text{Hex}$): 212–213 °C. IR (KBr): 1659, 1503, 1337, 1216 cm^{-1} . ^1H NMR (400 MHz, CDCl_3): δ 3.18 (s, 3H), 3.32 (s, 3H), 3.82 (s, 3H), 3.92 (s, 3H), 6.94 (s, 1H), 6.97 (s, 1H), 7.37 (d, $J=8.4$ Hz, 1H), 7.67 (dd, $J=1.6, 8.4$ Hz, 1H), 7.79 (s, 1H), 8.76 (d, $J=1.6$ Hz, 1H), 10.01 (s, 1H). ^{13}C NMR (100 MHz, CDCl_3): δ 34.0 (CH_3), 37.7 (CH_3), 55.6 (CH_3), 56.9 (CH_3), 109.7 (CH), 111.6 (C), 115.7 (CH), 116.8 (CH), 118.5 (C), 122.4 (CH), 123.5 (CH), 124.5 (C), 128.9 (C), 133.8 (C), 139.4 (C), 140.6 (CH), 149.7 (C), 150.8 (C), 184.0 (CH). HRMS ($\text{C}_{19}\text{H}_{19}\text{BrN}_2\text{NaO}_5\text{S}^+$): calcd. 489.0090 ($\text{M} + \text{Na}^+$), found 489.0098.

***N*-(4-Bromo-2,5-dimethoxyphenyl)-3-cyano-1-methyl-1H-indole-5-sulfonamide (49)**. Obtained as described in Method G1 from **47**. Yield: 19%. Brown crystals, m.p. (MeOH/acetone): 247.2–247.7 °C. IR (KBr): 3220, 3109, 2221, 1498, 1331, 1160, 690 cm^{-1} . ^1H NMR (400 MHz, CDCl_3): δ 3.65 (s, 3H), 3.86 (s, 3H), 3.88 (s, 3H), 6.88 (s, 1H), 7.12 (bs, 1H), 7.25 (s, 1H), 7.40 (d, $J=8.8$ Hz, 1H), 7.68 (s, 1H), 7.72 (dd, $J=1.6, 8.8$ Hz, 1H), 8.32 (d, $J=1.6$ Hz, 1H). ^{13}C NMR (100 MHz, CDCl_3): δ 33.7 (CH_3), 56.2 (CH_3), 56.7 (CH_3), 87.4 (C), 105.0 (CH), 105.9 (C), 110.7 (CH), 113.9 (C), 115.3 (CH), 120.2 (CH), 122.2 (CH), 125.5 (C), 126.8 (C), 132.6 (C), 137.4 (CH), 137.5 (C), 143.1 (C), 150.1 (C). HRMS ($\text{C}_{18}\text{H}_{16}\text{BrN}_3\text{NaO}_4\text{S}^+$): calcd. 471.9937 ($\text{M} + \text{Na}^+$), found 471.9943.

Tubulin polymerisation inhibition

Bovine brain tubulin was isolated as previously described¹⁷. The experiments were carried out with 1.0 mg/mL microtubular protein in pH 6.7 buffer (0.1 M MES, 1 mM EGTA, 1 mM MgCl_2 , 1 mM β -mercaptoethanol, 1.5 mM GTP) with or without the indicated ligands. The samples were incubated at 20 °C for 20 min, then cooled at 4 °C for 10 min. Tubulin polymerisation was measured by monitoring the turbidity increase observed at 450 nm when heating from 4 °C to 37 °C. After 20 min of stable readings, the temperature was switched back to 4 °C. Tubulin polymerisation inhibition percentage was referred to as the ratio between the amplitude obtained for the protein with ligand and the control curve. The compounds were first assayed at 10 μM and IC_{50} values were calculated for those that inhibited tubulin polymerisation by at least 50% in two independent experiments. SigmaPlot software

was used for calculations with monoexponential curves fitting the experimental data.

Cell culture conditions

Cell lines were purchased from ATCC. HeLa (human cervix epithelioid carcinoma) and HEK-293 (human embryonic kidney) cell lines were cultured at 37 °C in sub-confluent conditions under 95% humidified atmosphere and 5% CO_2 in Dulbecco's Modified Eagle Medium (DMEM) supplemented with 10% heat-inactivated FBS, 2 mM L-glutamine, 100 U/mL penicillin, 100 $\mu\text{g}/\text{mL}$ streptomycin, and 12.5 $\mu\text{g}/\text{mL}$ ciprofloxacin. HL-60 (human acute myeloid leukaemia) and HT-29 (human colorectal adenocarcinoma) cell lines were grown in RPMI 1640 supplemented with 10% heat-inactivated FBS, 2 mM L-glutamine, 100 U/mL penicillin, 100 $\mu\text{g}/\text{mL}$ streptomycin, and 12.5 $\mu\text{g}/\text{mL}$ ciprofloxacin in 95% humidified air and 5% CO_2 . AGS (human gastric adenocarcinoma) cell line was cultured under the same conditions using complete DMEM F-12. Cells were passaged at 80–90% confluency using 0.05% trypsin-EDTA and the culture medium was replaced every 2–3 days.

Cell proliferation assays

HeLa (1.5×10^3), HT-29 (3×10^3), HL-60 (5×10^3), AGS (10^3), and HEK-293 (4×10^3) cells were seeded in 96-well plates and incubated in the presence or the absence of the indicated compounds at concentrations ranging from 10^{-5} to 10^{-12} M. The cytostatic activity was measured after 72-h treatments using the XTT (sodium 3'-[1-(phenylaminocarbonyl)-3,4-tetrazolium]-bis(4-methoxy-6-nitro)-benzenesulfonic acid hydrate) cell proliferation kit (Roche Molecular Biochemicals; Mannheim, Germany) following the manufacturer's specifications. Each condition was seeded in triplicate, and experiments were repeated three times to calculate IC_{50} values using SigmaPlot software by non-linear regression curves fitting the data.

Cell cycle analysis

4×10^4 HeLa cells were seeded in six-well plates and incubated overnight before replacing the culture medium with fresh DMEM with or without the indicated compounds. Cells were harvested 24, 48, and 72 h following treatment, centrifuged, and fixed overnight in 70% ethanol at 4 °C. Cells were washed by centrifuging them twice with PBS, then dark incubated for 30 min with 0.2 mg/mL RNase A, 10 $\mu\text{g}/\text{mL}$ propidium iodide, and 0.5% NP-40 in PBS at room temperature. Samples were analysed with a CytomicsTM FC500 flow cytometer (Beckman-Coulter; Brea, CA, USA). Cell cycle analysis was carried out using Cyflogic software, quantifying apoptotic cell death as the percentage of cells in the SubG_0/G_1 peak (hypodiploid cells).

Confocal microscopy

8×10^4 HeLa cells were seeded on 0.01% poly-L-lysine pre-coated coverslips and incubated until 80% confluency. The culture medium was replaced with fresh DMEM, and cells were incubated in the presence or the absence of the indicated compounds for 24 h. After removing the medium, coverslips were washed three times with HPEM buffer (25 mM HEPES, 60 mM PIPES, 10 mM EGTA, 3 mM MgCl_2 , pH 6.6). Cells were fixed in 4% formaldehyde in HPEM buffer for 30 min and permeabilized in 0.5% Triton X-100 for 90 s at 4 °C. After four washes with HPEM buffer, cells were

incubated with Ab-1 anti- α -tubulin mouse monoclonal antibody (1:150 in PBS) (Invitrogen; Eugene, OR, USA) for 1 h at 4 °C. Cells were washed four times with PBS and incubated in the darkness with Ab-2 CY3-conjugated sheep anti-mouse IgG (1:100 in PBS) (Jackson ImmunoResearch; West Grove, PA, USA) for 1 h at 4 °C. After four washes with PBS, cell nuclei were stained with a drop of ProLong™ Gold antifade reagent with DAPI (Molecular Probes; Eugene, OR, USA), preserving the fluorescence. Samples were analysed by confocal microscopy using a Leica TC5 SP5 confocal microscope. Negative controls lacking the primary antibody and with an irrelevant primary antibody showed no fluorescence.

Docking experiments

The coordinates of 58 X-ray structures of tubulin in complex with different colchicine site ligands (pdb ID codes are given in the [Supplementary material](#)) were retrieved from the pbd²⁷. Chains C-E were removed along with all the water molecules and every ligand except the guanine nucleotides and their associated divalent cations. Five additional tubulin models were selected as previously described from representative clusters of the results of molecular dynamics simulations at 300 K using AMBER14²⁸ starting from the energy minimised coordinates of tubulin in complex with podophyllotoxin (pbd ID: 1SA1) and included in the docking experiments⁸. The resulting 63 tubulin dimer coordinates were aligned with DeepView v4.1²⁹ by superimposing their binding sites, represented by the residues closer to 8 Å to nodocazole and ABT-751 in their corresponding X-ray structures (pdb IDs 5CA1 and 3HKC, respectively). The 63 protein structures represent the known structural variation of the colchicine site of tubulin when in complex with structurally diverse ligands occupying the three subpockets and are therefore suited for ensemble docking. The ligands were built with Marvin v17.8³⁰ and prepared with Racoon³¹ and AutodockTools³². Docking of the virtual ligands onto each of the 63 protein models was performed with two docking programs using different scoring functions (AutoDock 4.2^{33,34} and PLANTS³⁵) in an attempt to better explore the binding geometries and energies. AutoDock 4.2 was run with the Lamarckian genetic algorithm (LGA) 100–300 times with a maximum of 2.5×10^6 energy evaluations, 150 individuals in the population, and a maximum of 27,000 generations, and PLANTS³⁵ was run using the lowest speed and the chemPLP scoring function. The binding poses were automatically classified by the binding pockets they occupy, and the results were tabulated using KNIME^{36,37} pipelines and in-house scripts. File format conversions were performed with Unicon³⁸. The binding energies were automatically converted to z-scores and compared. The results were analysed with Chimera³⁹, AutoDockTools^{33,34}, Marvin³⁰, OpenEye⁴⁰, and JADOPPT⁴¹. Docking poses were selected if they were found by the two docking programs in the two first quartiles and above any alternative based on the combined z scoring. Additionally, the docked poses have been re-scored using a MM-PBSA approximation with AMBER as described by Graves⁴² and implemented in DOCK6.9⁴³.

Molecular dynamics simulations

Fully solvated molecular dynamics simulations were performed to ascertain the stability of the proposed poses for compounds **5**, **9**, and **16**, as previously described¹⁹. The initial configurations for the molecular dynamics simulations were extracted from the docking results. Briefly, all MD simulations were carried out with the AMBER11⁴⁴ program using the ff10 force-field parameters for the protein^{45,46}, the gaff for the ligand⁴⁷, a set of parameters

developed for a better thermodynamic description of guanine nucleotides and Mg²⁺ ions⁴⁸, the Joung and Cheatham parameters for non-polarizable spherical ions^{49,50}, and TIP3P for water molecules⁵¹. The initial confirmation from the docking experiments was simulated with periodic boundary conditions in a truncated octahedron box with roughly 30,000 TIP3P water molecules surrounding the solute by at least 10 Å until the faces and with Na⁺ ions added to compensate the solute charges. The system was initially relaxed by energy minimisation with harmonic restraints on the positions of the solute heavy atoms followed by unrestricted energy minimisation. Subsequently, it was heated to 300 K and equilibrated for 200 ns, and then subjected to production molecular dynamics simulations for 1000 ns using an isothermal–isobaric ensemble and a 2 fs time-step. The trajectories were analysed by means of the ptraj program within AMBER and visualised with VMD^{52,53}.

Results and discussion

Chemistry

The indolesulfonamides were prepared by first assembling the *N*-formylindolinesulfonamides (**2**, **19**, and **33**) followed by formyl to methyl reduction (**3**, **20**, and **34**) and aromatisation to the corresponding indoles (**4**, **21**, and **35**) (Scheme 1). Structural modifications on main scaffolds were thereafter introduced by combinations of aromatic substitution reactions, alkylations of the sulfonamide nitrogen, and functional group transformations.

Alkylations of the sulfonamide nitrogen were carried out under basic catalysis to form the sulfonamide anion, which reacts with alkylating agents leading to methyl (**5**, **13**, **22**, **36**, **41**, **46**), ethyl (**6**, **14**, **23**), acetate (**7**, **24**, **37**), acetonitrile (**9**, **25**, **38**), and benzyl (**26**, **27**, **39**) substituted sulfonamides. Saponification of the ethyl ester **7** gave carboxylic acid **8**.

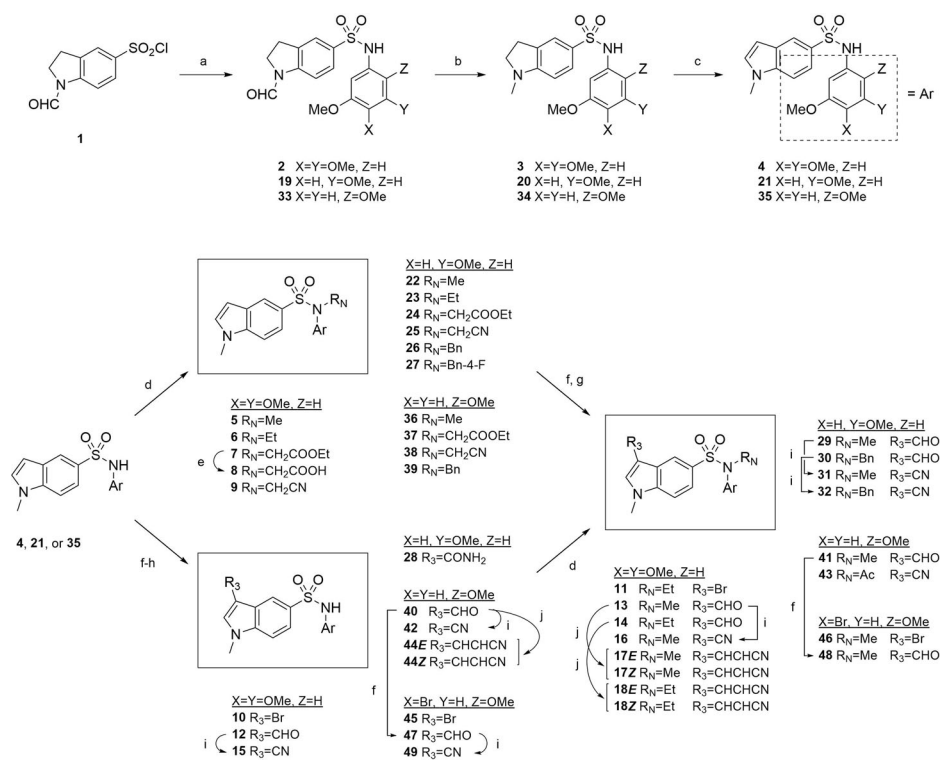
Brominations with NBS occurred preferentially at the indole 3-position when unsubstituted (**10**, **11**) and at the *para* position to the aniline nitrogen of the other aryl group when it is already substituted (**45**, **47**, **48**). Formylations of the indole 3-position were carried out with good yields under Vilsmeier–Haack conditions⁵⁴ (**12**, **29**, **30**, **40**). The aldehydes were converted into nitriles (**15**, **16**, **31**, **32**, **42**, **43**, **49**) by transforming them first into the corresponding oximes followed by thermal elimination of the resulting acetates in refluxing acetic anhydride^{18,55,56}. Treatment of 3-formylindoles in basic acetonitrile gave the Knoevenagel adducts (**17E/Z**, **18E/Z**, and **44E/Z**). The amide **28** was prepared upon the reaction of sulfonamide **21** with CSI⁵⁷.

All these modifications allowed us to assay a wide variety of new potential ligands to explore the contribution of the chemical structure to the anti-tumour activity.

Indolesulfonamides exert potent anti-proliferative activity

The effect of the synthesised compounds on the *in vitro* cell viability was measured following the XTT procedure¹⁷. Four human tumour cell lines were assayed, namely HeLa cervix epithelioid carcinoma, HT-29 colon adenocarcinoma, HL-60 acute myeloid leukaemia, and AGS gastric adenocarcinoma, as well as the non-tumorigenic cell line HEK-293 from human embryonic kidney tissue. The results for half-maximal inhibitory concentrations (IC₅₀) are summarised in Table 1.

Indolesulfonamides exerted anti-proliferative activity with IC₅₀ values in the submicromolar range, displaying akin potencies against the four tumour cell lines, although HT-29



Scheme 1. Synthesis of indolesulfonamides. Reagents and conditions: (a) Ar-NH₂, NaHCO₃, EtOAc/water, rt, 4–14 h, N₂. (b) NaBH₄, trichloroacetic acid, THF, 4 °C-rt, 4–72 h, N₂. (c) DDQ, THF, 4 °C-rt, 18–24 h, N₂. (d) Halogen-R_N, KOH/CH₃CN or K₂CO₃/DMF, rt, 3 h-10 days. (e) KOH, MeOH, rt, 30 min. (f) NBS, CH₂Cl₂, 4 °C, 15 min-24 h, N₂. (g) i) POCl₃, DMF, 4 °C, 30 min, N₂; ii) indole derivative, 4 °C, 5 min-1 h, N₂. (h) CS₂, 1,2-dichloroethane, 4 °C-rt, 24 h, N₂. (i) i) NH₂OH·HCl, pyr, MeOH, reflux, 12–48 h, N₂; ii) Ac₂O, pyr, 130 °C, 30–96 h, N₂. (j) KOH, CH₃CN, rt, 7 days.

adenocarcinoma is slightly more resistant, consistently with the previous reports¹⁸. Many of them showed higher potency than ABT-751, and **5** displayed IC₅₀ values (2.4, 4.3, and 1.1 nM against HeLa, HT-29, and HL-60, respectively) better than those of CA-4 (3, 32, and 13 nM against HeLa, HT-29, and HL-60, respectively). The comparison of indolesulfonamides with other indole analogues just differing in the bridge connecting the two aryl groups, such as indolecombretastatins (**V-VIII**)^{17,18}, or indoleisocombretastatins (**XIII**)¹⁹, shows that when the indole 3-position is unsubstituted the sulfonamides and the isocombretastatins are more potent anti-proliferative agents than the combretastatin analogues (**V** vs. **4-7** and **9**).

Substitutions at the indole 3-position greatly improve the anti-proliferative potencies in indolecombretastatins^{17,18} and moderately so in indoleisocombretastatins¹⁹ but were not favourable for indolesulfonamides (Supplemental Figure 1, SF1). Formyl groups (**12-14**) cause roughly a 10 to 20-fold potency reduction with respect to their unsubstituted pairs (e.g. compare 41.2, 385.2, 89.3, and 35.3 nM for formylated **13** against HeLa, HT-29, HL-60, and AGS, respectively vs. 2.4, 4.3, 1.1, and 3.3 nM, respectively for its unsubstituted analogue **5**), the same trend observed for indolecombretastatins. Bromine substituents (**10, 11, 45**, and **46**) cause a 2 to 6-fold potency reduction (e.g. compare 10.8, 51.0, 10.9, and 12.9 nM for **4** against HeLa, HT-29, HL-60, and AGS, respectively vs. 48.2, 249.9, 28.0, and 78.9 nM, respectively for its brominated analogue **10**), with similar IC₅₀ values to the equivalent combretastatins (**VIII** vs. **10, 11**). Nitrile derivatives (**15, 16**) are the most potent amongst the substituted indolesulfonamides (21.4, 55.2, 16.2, and 11.2 nM for **15** against HeLa, HT-29, HL-60, and AGS, respectively and 12.3, 51.9, 20.1, and 19.4 nM, respectively for **16**),

although less than their combretastatin and isocombretastatin pairs (**VII** and **XIII**, R₃ = CN respectively). Larger substituents, such as the propanenitriles, led to IC₅₀ values akin to those observed for aldehyde groups (e.g. compare 35.4, 78.3, 14.4, and 11.2 nM for the *E*-propanenitrile **17E** against HeLa, HT-29, HL-60, and AGS, respectively vs. 41.2, 385.2, 89.3, and 35.3 nM, respectively, for formylated **13**), except for the 2,5-dimethoxyphenyl ring (**44E, 44Z**) where they cause a potency increase. The activity of the *E* isomers was slightly higher than *Z* isomers.

Overall, structures with a 3,4,5-trimethoxyphenyl ring displayed approximately an order of magnitude lower IC₅₀ values than those with a 3,5-dimethoxyphenyl moiety, which, in turn, showed better results than 2,5-dimethoxyphenyl derivatives (e.g. compare 2.4, 4.3, 1.1, and 3.3 nM for the 3,4,5-trimethoxyphenylated **5** against HeLa, HT-29, HL-60, and AGS, respectively vs. 20.1, 42.6, 23.5, and 30.5 nM, respectively for **22** with a 3,5-dimethoxyphenyl ring, and 169.2, 613.1, 233.8, and 149.5, respectively for **36**, with a 2,5-dimethoxyphenyl ring). This observation is in agreement with previous structure-activity relationship (SAR) reports revealing the 3,4,5-trimethoxyphenyl ring as pivotal for high tubulin inhibition and anti-proliferative potency⁵⁸, although diphenylsulfonamides are more tolerant to A ring variations², and a 2,4,5-trisubstituted phenyl A ring has been shown to be a successful replacement for the 3,4,5-trimethoxyphenyl ring⁵⁹.

Substitutions of the sulfonamide hydrogen with methyl groups greatly increased the cytotoxic potency (e.g. compare 10.8, 51.0, 10.9, and 12.9 nM for unsubstituted sulfonamide **4** against HeLa, HT-29, HL-60, and AGS, respectively vs. 2.4, 4.3, 1.1, and 3.3 nM, respectively for methylated **5**). Ethyl and acetonitrile moieties also made a significant improvement for the series with less bulky A

Table 1. Biological evaluation of indolesulfonamides.

No.	R ₃	R _N	Ar	Anti-proliferative activity (nM)				
				HeLa	HT-29	HL-60	AGS	HEK-293
4	H	H	3,4,5-(MeO) ₃ -Ph	10.8 ± 3.4	51.0 ± 7.8	10.9 ± 4.9	12.9 ± 4.2	6.4 ± 1.0
5	H	Me	3,4,5-(MeO) ₃ -Ph	2.4 ± 0.4	4.3 ± 0.9	1.1 ± 1.0	3.3 ± 0.8	2.3 ± 0.4
6	H	Et	3,4,5-(MeO) ₃ -Ph	22.1 ± 5.8	14.4 ± 8.2	10.8 ± 4.7	8.2 ± 4.5	6.0 ± 1.1
7	H	CH ₂ COOEt	3,4,5-(MeO) ₃ -Ph	28.8 ± 7.3	53.3 ± 8.9	15.2 ± 2.6	26.5 ± 7.8	6.6 ± 2.1
8	H	CH ₂ COOH	3,4,5-(MeO) ₃ -Ph	>1000	>1000	>1000	n.d.	n.d.
9	H	CH ₂ CN	3,4,5-(MeO) ₃ -Ph	13.7 ± 3.5	47.7 ± 5.2	26.7 ± 7.5	5.6 ± 1.8	5.1 ± 2.8
10	Br	H	3,4,5-(MeO) ₃ -Ph	48.2 ± 4.9	249.9 ± 46.3	28.0 ± 5.0	78.9 ± 8.4	24.1 ± 6.5
11	Br	Et	3,4,5-(MeO) ₃ -Ph	30.0 ± 5.9	52.8 ± 8.2	24.1 ± 8.9	53.1 ± 2.6	24.1 ± 6.5
12	CHO	H	3,4,5-(MeO) ₃ -Ph	206.5 ± 38.6	623.8 ± 140.6	209.8 ± 83.9	213.2 ± 33.6	229.4 ± 22.3
13	CHO	Me	3,4,5-(MeO) ₃ -Ph	41.2 ± 4.9	385.2 ± 48.2	89.3 ± 14.0	35.3 ± 3.6	39.9 ± 5.6
14	CHO	Et	3,4,5-(MeO) ₃ -Ph	178.5 ± 60.6	606.4 ± 84.7	123.2 ± 89.1	157.8 ± 22.3	175.7 ± 23.5
15	CN	H	3,4,5-(MeO) ₃ -Ph	21.4 ± 2.7	55.2 ± 11.8	16.2 ± 6.3	11.2 ± 1.7	13.8 ± 1.4
16	CN	Me	3,4,5-(MeO) ₃ -Ph	12.3 ± 4.0	51.9 ± 9.8	20.1 ± 8.3	19.4 ± 5.8	6.8 ± 19.6
17E	CHCHCN	Me	3,4,5-(MeO) ₃ -Ph	35.4 ± 7.6	78.3 ± 15.7	14.4 ± 9.0	18.0 ± 1.2	9.7 ± 0.5
17Z	CHCHCN	Me	3,4,5-(MeO) ₃ -Ph	44.6 ± 8.5	107.1 ± 15.6	23.0 ± 9.6	22.6 ± 1.5	11.4 ± 1.0
18E	CHCHCN	Et	3,4,5-(MeO) ₃ -Ph	68.6 ± 15.1	342.3 ± 48.8	120.4 ± 69.1	162.8 ± 18.3	156.0 ± 15.6
18Z	CHCHCN	Et	3,4,5-(MeO) ₃ -Ph	188.0 ± 27.7	336.3 ± 47.6	258.0 ± 47.7	196.6 ± 29.9	161.5 ± 19.6
21	H	H	3,5-(MeO) ₂ -Ph	1401.8 ± 188.8	>1000	>1000	n.d.	n.d.
22	H	Me	3,5-(MeO) ₂ -Ph	20.1 ± 2.7	42.6 ± 7.8	23.5 ± 5.0	30.5 ± 3.9	11.8 ± 3.0
23	H	Et	3,5-(MeO) ₂ -Ph	55.2 ± 8.3	153.6 ± 17.7	41.0 ± 6.8	263.0 ± 44.6	87.8 ± 5.9
24	H	CH ₂ COOEt	3,5-(MeO) ₂ -Ph	320.7 ± 24.2	593.4 ± 30.9	328.3 ± 26.8	529.8 ± 37.6	431.8 ± 50.0
25	H	CH ₂ CN	3,5-(MeO) ₂ -Ph	68.6 ± 8.7	230.8 ± 20.6	104.7 ± 6.8	199.6 ± 31.0	111.5 ± 30.0
26	H	Bn	3,5-(MeO) ₂ -Ph	273.2 ± 20.0	369.6 ± 35.2	246.8 ± 26.4	266.9 ± 40.3	177.0 ± 42.5
27	H	Bn-4-F	3,5-(MeO) ₂ -Ph	278.6 ± 22.4	326.8 ± 76.0	229.2 ± 43.2	207.4 ± 20.1	222.0 ± 96.1
28	CONH ₂	H	3,5-(MeO) ₂ -Ph	1770.2 ± 546.6	1504.7 ± 598.7	>1000	n.d.	n.d.
29	CHO	Me	3,5-(MeO) ₂ -Ph	>1000	>1000	>1000	n.d.	n.d.
30	CHO	Bn	3,5-(MeO) ₂ -Ph	>1000	>1000	>1000	n.d.	n.d.
31	CN	Me	3,5-(MeO) ₂ -Ph	551.4 ± 21.2	713.0 ± 30.8	512.8 ± 18.3	433.8 ± 90.6	573.7 ± 38.3
32	CN	Bn	3,5-(MeO) ₂ -Ph	794.3 ± 34.4	993.0 ± 74.6	754.5 ± 33.9	789.4 ± 71.5	680.5 ± 55.8
35	H	H	2,5-(MeO) ₂ -Ph	320.2 ± 49.0	898.0 ± 92.6	262.2 ± 67.5	454.1 ± 49.2	451.5 ± 47.8
36	H	Me	2,5-(MeO) ₂ -Ph	169.2 ± 34.0	613.1 ± 82.2	233.8 ± 37.0	149.5 ± 20.4	126.9 ± 11.4
37	H	CH ₂ COOEt	2,5-(MeO) ₂ -Ph	1020.2 ± 30.1	>1000	>1000	n.d.	n.d.
38	H	CH ₂ CN	2,5-(MeO) ₂ -Ph	220.5 ± 99.1	435.4 ± 81.7	160.4 ± 81.3	247.3 ± 36.5	182.8 ± 32.3
39	H	Bn	2,5-(MeO) ₂ -Ph	818.0 ± 68.4	948.4 ± 41.0	899.7 ± 53.5	840.9 ± 53.1	584.0 ± 83.7
40	CHO	H	2,5-(MeO) ₂ -Ph	>1000	>1000	>1000	n.d.	n.d.
41	CHO	Me	2,5-(MeO) ₂ -Ph	>1000	>1000	>1000	n.d.	n.d.
42	CN	H	2,5-(MeO) ₂ -Ph	~1000	>1000	>1000	n.d.	n.d.
43	CN	Ac	2,5-(MeO) ₂ -Ph	>1000	>1000	>1000	n.d.	n.d.
44E	CHCHCN	H	2,5-(MeO) ₂ -Ph	319.5 ± 49.1	545.8 ± 85.6	250.6 ± 59.6	786.0 ± 53.7	854.1 ± 52.5
44Z	CHCHCN	H	2,5-(MeO) ₂ -Ph	469.0 ± 54.1	775.9 ± 143.1	400.7 ± 105.8	885.2 ± 35.6	990.2 ± 51.0
45	Br	H	4-Br-2,5-(MeO) ₂ -Ph	369.0 ± 91.9	343.4 ± 65.5	155.7 ± 83.4	410.4 ± 49.1	393.7 ± 72.1
46	Br	Me	4-Br-2,5-(MeO) ₂ -Ph	273.5 ± 27.8	417.6 ± 64.7	203.7 ± 97.4	210.7 ± 32.3	354.9 ± 88.2
47	CHO	H	4-Br-2,5-(MeO) ₂ -Ph	>1000	>1000	>1000	n.d.	n.d.
48	CHO	Me	4-Br-2,5-(MeO) ₂ -Ph	765.3 ± 102.7	611.5 ± 120.9	206.6 ± 90.2	518.3 ± 34.8	502.5 ± 22.8
49	CN	H	4-Br-2,5-(MeO) ₂ -Ph	320.2 ± 72.5	417.2 ± 87.0	329.1 ± 56.3	~1000	>1000
CA-4 ¹				3	32	13		
ABT-751				388	514			

Anti-proliferative activity exerted by the compounds against human tumour cell lines (HeLa, HT-29, HL-60, and AGS) and the non-tumorigenic human cell line HEK-293. IC₅₀ values were determined after 72 h incubations and are expressed in nanomolar units.

rings (e.g. compare all larger than 1 µM for unsubstituted 3,5-dimethoxyphenylsulfonamide **21** against HeLa, HT-29, HL-60, and AGS vs. 55.2, 153.6, 41.0, and 263.0 nM, respectively for ethylated **23**, and 68.6, 230.8, 104.7, and 199.6, respectively for **25**, with acetonitrile on the sulfonamide and a 3,5-dimethoxyphenyl ring), but not for the 3,4,5-trimethoxyphenyl one (e.g. compare 10.8, 51.0, 10.9, and 12.9 nM for unsubstituted sulfonamide **4** against HeLa, HT-29, HL-60, and AGS respectively vs. 22.1, 14.4, 10.8, and 8.3 nM, respectively for ethylated **6**, and 13.7, 47.7, 26.7, and 5.6, respectively for sulfonamidoacetonitrile **9**). The improved potency of these larger substituents on the sulfonamide has been attributed to a different binding mode for *N*-(2,4,5-trisubstitutedphenyl) benzenesulfonamides⁵⁹, and is consistent with the results here obtained. Even bulkier substitutions such as the acetates or the benzyls were less favourable.

Indolesulfonamides are not MDR substrates

We have previously reported that pre-treatment with the non-selective MDR inhibitor verapamil remarkably increased the potency of some indolecambretastatins such as **VI** (100-fold) and **VII** (10-fold) against A-549 human lung carcinoma cells¹⁸. In order to test whether these novel indolesulfonamides are substrates of MDR efflux pumps, the cytotoxicity of the indolesulfonamides against HeLa cells pre-treated with verapamil at 1 µM and 10 µM or the MDR1 selective inhibitor elacridar at 100 nM were compared with the values in the absence of the inhibitors (cf. Table 1 and Supplemental Table 1). The MDR inhibitors showed no effect in cell proliferation at the assayed concentrations. No differences were observed between the treatments with the selective MDR1 inhibitor elacridar and the pleiotropic agent verapamil, thus suggesting that the effects of verapamil treatments are due as well to inhibition of the MDR transporter.

Table 2. Effect of indolesulfonamides on tubulin polymerisation *in vitro* and the cell cycle.

No.	TPI		G ₂ /M arrest		
	%	IC ₅₀	10 nM	100 nM	1 μM
4	43	—	—	+	+
5	100	2.1	+	+	+
6	96	2.2	+/-	+	+
7	86	4.2	—	+	+
8	22	—	—	—	—
9	56	9.7	—	+	+
10	42	—	—	+	+
11	68	5.4	—	+	+
12	13	—	—	—	+
13	19	—	—	+	+
14	9	—	—	—	+
15	24	—	—	+	+
16	52	10.0	—	+	+
17E	99	5.6	—	+	+
17Z	56	8.8	—	+	+
18E	74	6.3	—	+	+
18Z	26	—	—	+	+
21	0	—	—	—	—
22	10	—	—	+	+
23	16	—	—	+	+
24	14	—	—	—	+
25	11	—	—	+/-	+
26	13	—	—	—	+
27	24	—	—	—	+
28	0	—	—	—	—
29	2	—	—	—	—
30	14	—	—	—	—
31	13	—	—	—	+
32	15	—	—	—	+
35	6	—	—	—	+
36	20	—	—	+/-	+
37	4	—	—	—	—
38	16	—	—	+/-	+
39	11	—	—	—	+
40	0	—	—	—	—
41	0	—	—	—	—
42	0	—	—	—	—
43	0	—	—	—	—
44E	25	—	—	—	+
44Z	8	—	—	—	+
45	32	—	—	—	+
46	55	10.1	—	+/-	+
47	8	—	—	—	—
48	43	—	—	—	+
49	12	—	—	—	+

Tubulin polymerisation inhibition percentage (TPI) was evaluated at 10 μM and half-maximal inhibitory concentration (IC₅₀) was determined for those compounds inhibiting tubulin polymerisation by at least 50% and expressed in micromolar units. The G₂/M arrest was evaluated in HeLa cells at 10 nM, 100 nM, and 1 μM and indicated qualitatively based on the percentage of cells in the G₂/M population after 24 h treatments. n.d. = not determined; + = >50%; ± = 35–50%; — = no effect (G₂/M population in untreated samples = 25%).

The changes in cytotoxicity values for indolesulfonamides caused by the MDR inhibitors are small, typically within 2-fold (Supplemental Table 1, ST1). Only the ethyl derivative **6** displayed 7- to 11-fold improvement in its efficiency with the inhibition of MDR-mediated transport (22.1 nM against HeLa vs. 2.3, 3.0, and 2.7 for the co-treatments with 0.1 μM elacridar, 1 μM verapamil, and 10 μM verapamil, respectively), clearly indicating that it is a substrate of MDR efflux. Upon co-treatment with the MDR inhibitors, this compound is equally potent against HeLa as **5** (2.4 nM), the most potent compound of the series, thus indicating that the potency difference observed between the *N*-methyl- and the *N*-ethylsulfonamides is caused by drug efflux and not by interaction with the target. On the other hand, the acetonitriles are not substrates of the MDR proteins, and their lower potency might be caused by a less favourable interaction with tubulin.

Overall, the series with 3,4,5-trimethoxyphenyl rings is the most affected by MDR inhibition, with 8 compounds (**6**, **7**, **10**, **11**, **17E/Z**, **18E/Z**) with increased potencies out of 16 active, compared to the 2,5-dimethoxyphenyl (one compound, **46**) and the 3,5-dimethoxyphenyl series (none). Considering that MDR efflux is an important means of resistance to anti-tumour therapies⁶⁰, the lower susceptibility of these alternative series is an interesting property.

The compounds that show reductions in the IC₅₀ values in the presence of MDR inhibitors and can be considered as efflux pump substrate candidates usually carry bulkier and more hydrophobic groups than the non-substrates (Supplemental Table 1, ST1), as is the case for the trimethoxyphenyl ring or the addition of lipophilic groups such as bromines or propenenitriles. Fortunately, none of the most active compounds within each series (**5**, **22**, **35**) seemed to be good MDR substrates, in contrast with the structurally related indolecambretastatin¹⁸. The replacement of the olefin bridge by a sulfonamide moiety apparently reduces this liability, as neither the aldehyde nor the nitrile derivatives are exported, which is an advantage for the diarylsulfonamides over the cambretastatin.

Indolesulfonamides act on tubulin polymerisation

The synthesised compounds were assayed for polymerisation inhibition of the microtubule protein *in vitro*¹⁷ to determine whether the cytotoxic profile is related to tubulin targeting activity (Table 2). The tubulin polymerisation inhibition (TPI) and the anti-proliferative activity follow similar trends, therefore finding similar SARs. All the compounds with TPI IC₅₀ values lower than 10 μM showed anti-proliferative values under 100 nM, although the opposite is not always true (e.g. **10**, **13**, **15**, or **22**). This apparent inconsistency has been previously observed and explained by the fact that it is disruption of polymerisation dynamics which causes the anti-proliferative effect and not the microtubule mass alteration that occurs at higher concentrations, although both effects are often associated in some structural families. MDR1 inhibition with elacridar or verapamil further increases the similarity, thus suggesting that resistance mediated by efflux pumps acts as a confounding factor for the correlation between anti-proliferative and TPI potencies. Accordingly, similar to what is observed for the cytotoxic activity, the 3,4,5-trimethoxyphenyl series exhibited TPI values better than the 3,5-dimethoxyphenyl and 2,5-dimethoxyphenyl series. Substitutions at the sulfonamide nitrogen increased TPI (e.g. **5–7** and **9** versus **4**) and modifications at the indole 3-position were detrimental, leading to 3- to 5-fold higher IC₅₀ values when the indole ring of **5** (IC₅₀ = 2.1 μM) was substituted, as for compounds **16** and **17E/Z** (IC₅₀ = 10.0, 5.6, and 8.8 μM, respectively). Since both SARs led to the same conclusions, the tubulin polymerisation inhibition could be the putative mechanism of action of the anti-proliferative response. Compounds **5** and **6** displayed TPI IC₅₀ values of 2.1 and 2.2 μM, respectively, proving more potent than CA-4 (IC₅₀ = 3 μM) and akin to the indolecambretastatin analogue **V** (IC₅₀ = 2.0 μM). However, these very similar tubulin polymerisation inhibition values do not go in parallel with their anti-proliferative effects. This could be explained by an MDR mechanism acting on **V** or by a different TPI to cytotoxicity ratio in different structural series, as previously observed. The same trend was observed for **VIII**, which displayed remarkably increased TPI than **10** and **11** despite showing lower cytotoxic activity, whereas even higher potency in TPI, such as **VI** and **VII**, was needed for comparable cytotoxicity values.

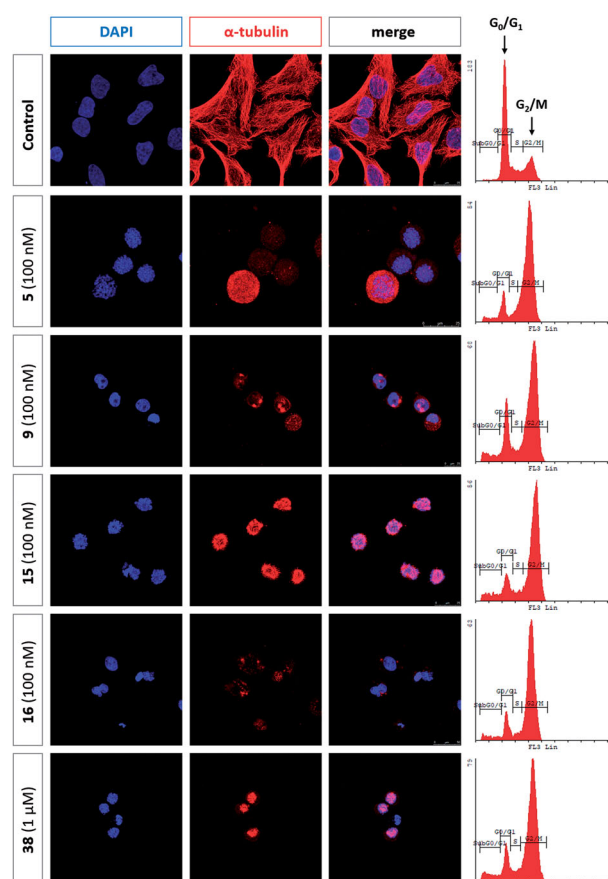


Figure 2. Effect of compounds **5**, **9**, **15**, **16**, and **38** on the microtubule network and cell cycle in HeLa cells. Cells were incubated in the absence (control) or the presence of the selected compounds for 24 h, fixed, and processed. Nuclei (DAPI, blue fluorescence) and the microtubule network (α -tubulin, red fluorescence) were analysed by confocal microscopy. Scale bar: 25 μ m (except **16**: 50 μ m). The cell cycle profiles were also analysed in parallel by flow cytometry. The photomicrographs and cell cycle histograms are representative of at least three independent experiments.

Indolesulfonamides, therefore, trigger an enhanced cytotoxic response with akin TPI to analogous indolecombretastatins.

The effect of the compounds on the microtubule system of HeLa cells was studied by immunofluorescence imaging of tubulin (Figure 2). Treatment with the compounds for 24 h to allow for maximal effect on the microtubular system at minimal cell death (see later the effects on the cell cycle) results in cells lacking the hairy microtubule skeleton typical of untreated HeLa cells (red fluorescence). This loss of the microtubule fibres comes along with round-shaped cell morphology and with the appearance of multilobulated nuclei, both consistent with the observed impairment of microtubule assembly. These results support a tubulin inhibition-mediated mechanism of action.

Indolesulfonamides arrest cells in mitosis and induce apoptotic cell death

The effect of the compounds on the cell cycle distribution in HeLa cells was evaluated at three different concentrations (10 nM, 100 nM, and 1 μ M) after incubations of 24, 48, and 72 h. The percentages of cells gathered in SubG₀/G₁ and G₂/M populations are listed in Supplemental Table 2 (ST2) and the results for G₂/M arrest summarised in Table 2. The compounds that proved effective in the proliferation assay also induced a sustained increase in the percentage of cells in G₂/M compared to control conditions,

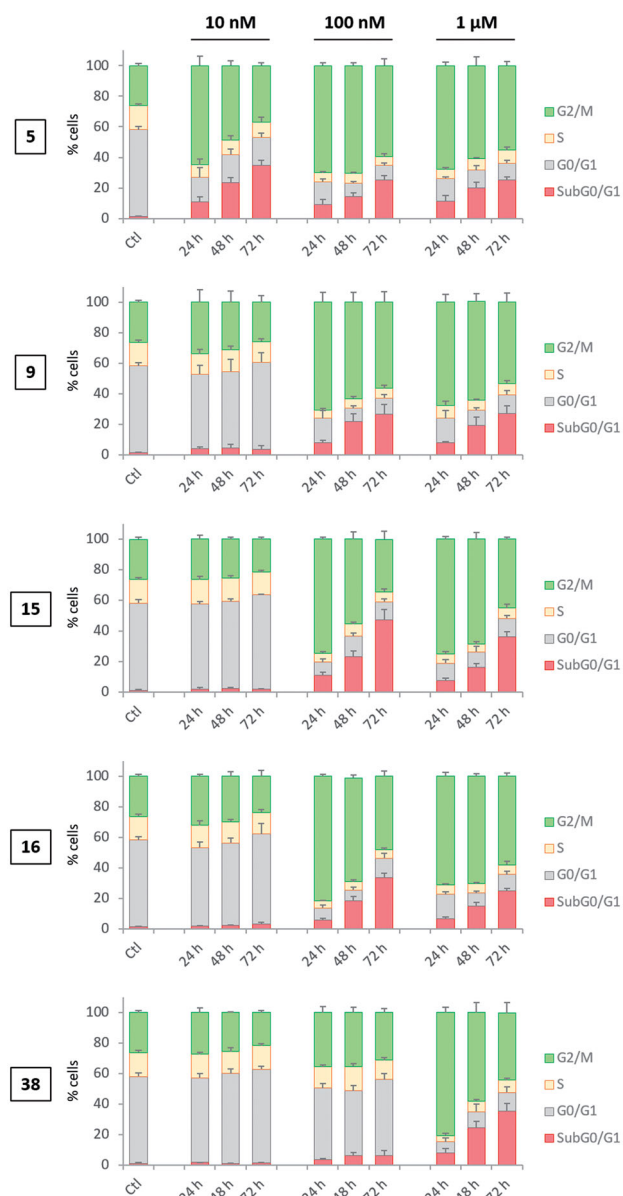


Figure 3. Analysis of cell cycle populations (SubG₀/G₁, G₀/G₁, S, and G₂/M) in HeLa cells after treatment with the indicated compounds for 24, 48, and 72 h at 10 nM, 100 nM, and 1 μ M. The results are expressed in bars as mean \pm SD.

which is in line with the proposed mechanism of action, as microtubule dynamics disruption leads to a halt in mitosis³. Compounds with IC₅₀ values against HeLa cells around 10⁻⁷ M caused mitotic blockage at 1 μ M (e.g. **12**), whereas for potencies around 10⁻⁸ M, the alteration on the time-course was also manifested at 100 nM (e.g. **15**) (Figure 3). These observations point out that cell proliferation inhibition is closely related to cell division arrest. Compound **5**, which is the most potent one regarding proliferation assays (Table 1), triggered an accumulation of cells in G₂/M even at 10 nM (63.6% at 24 h) compared to untreated HeLa cells (21.7%). Compound **6** also showed partial effects at that concentration (data not shown), as expected for a lower accumulation within the cell due to MDR efflux. For the indolesulfonamides substituted at the indole 3-position, the more potent ones are those with a cyano group, that arrest cells in the G₂/M phases at concentrations as low as 100 nM (**15** and **16**), in agreement with the cell proliferation inhibitory studies, with similar results for unsubstituted and methylated sulfonamide bridges (**15** vs. **16**).

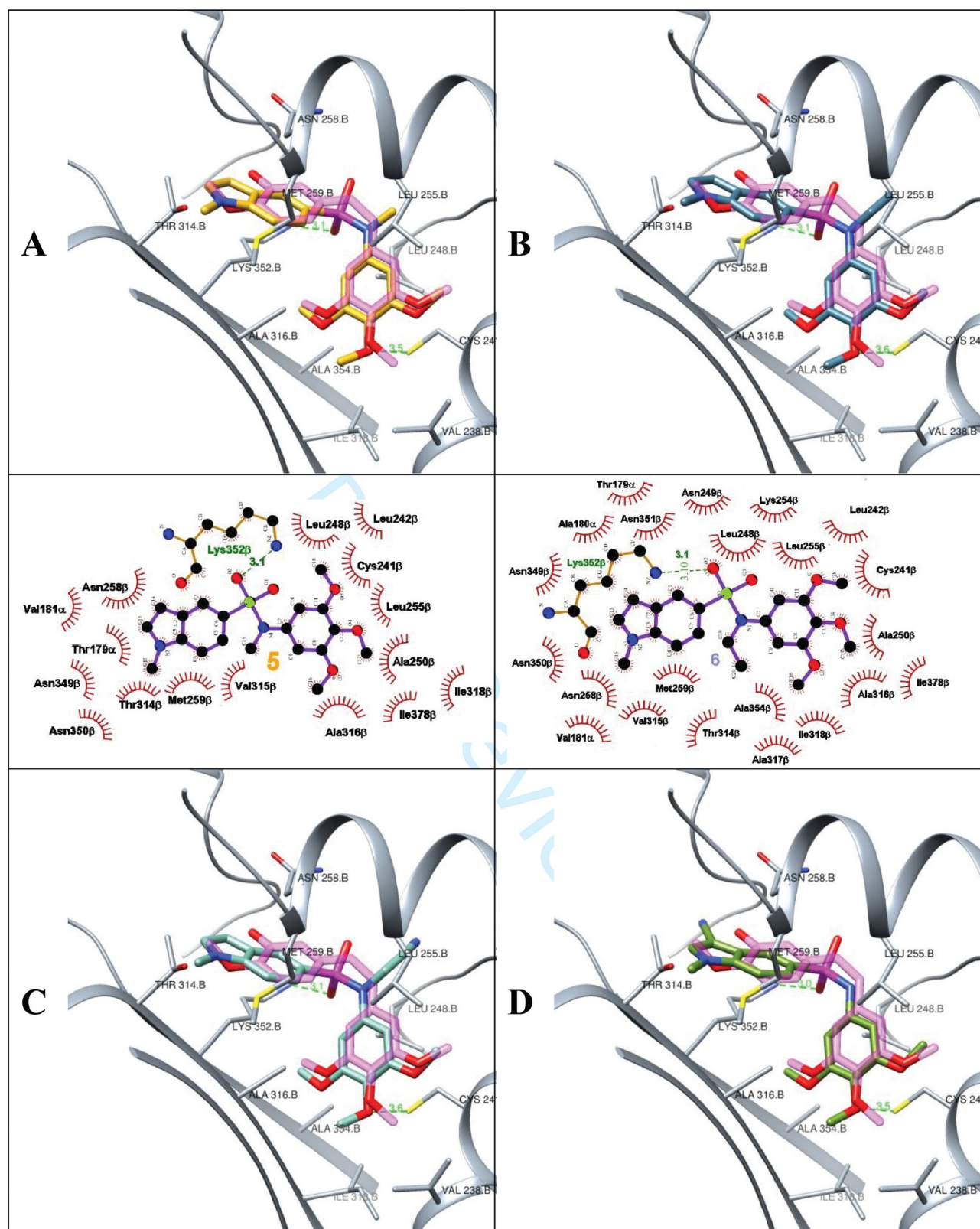


Figure 4. 3D structural models (up) and 2D diagrams⁶⁴ (down) of the complexes of compounds **5** (A, carbons in mustard), **6** (B, carbons in steel blue), **9** (C, carbons in sky blue), **15** (D, carbons in olive green), **16** (E, carbons in black) and **38** (F, carbons in lavender) at the colchicine site of tubulin, represented in their respective consensus poses. The protein is shown in pigeon blue cartoons and contacting sidechains are shown and labelled. The X-ray structure of combretastatin A-4 in complex with tubulin is superimposed in transparent pink to easy structural comparisons.

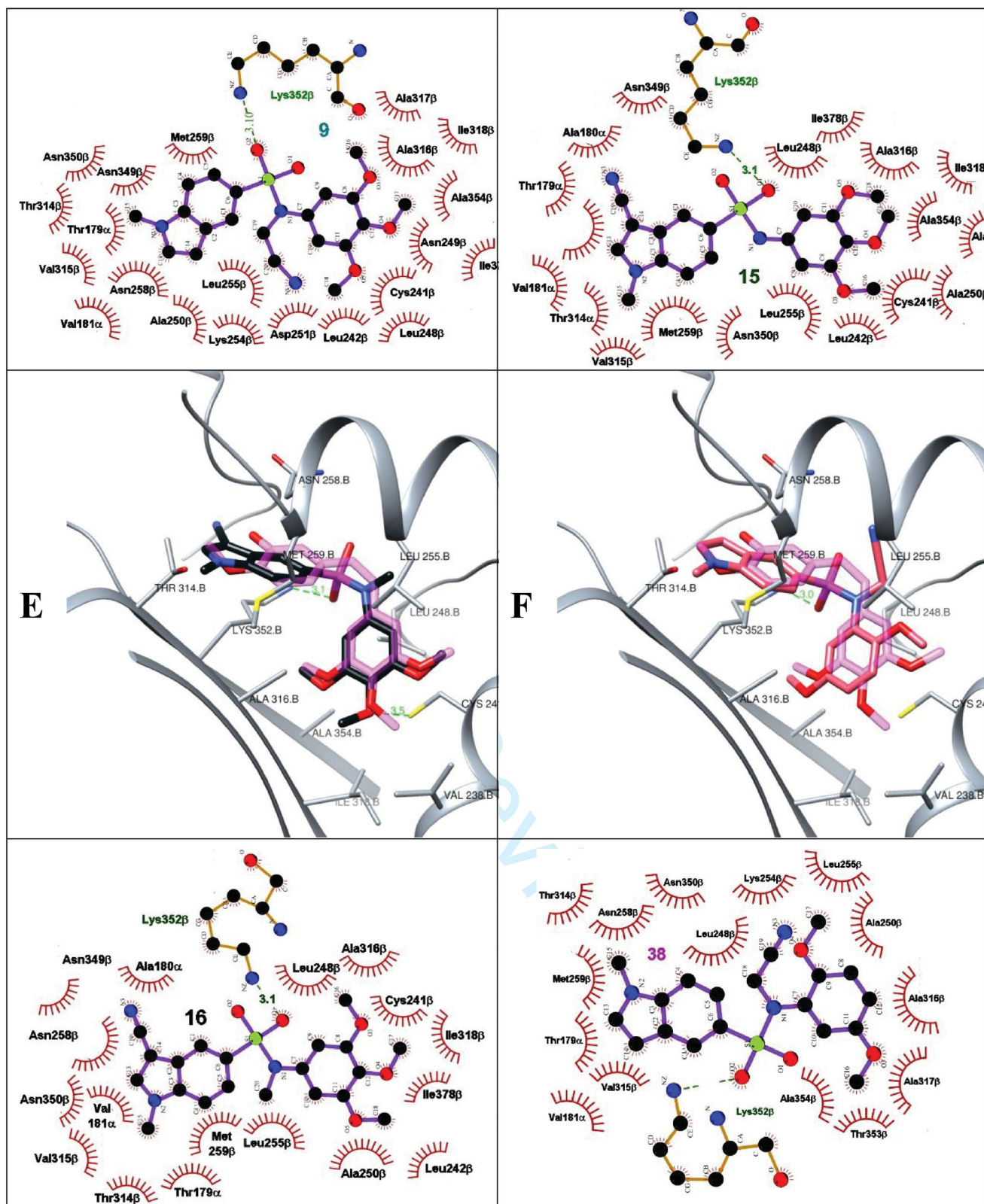


Figure 4. Continued.

The effect of representative compounds on the cell cycle distribution of the non-tumorigenic HEK-293 cells was also determined to analyse potential differences between tumour versus non-tumorigenic cell lines. Cell death induction was consistently delayed in comparison with HeLa cells (data not shown), which might result in a favourable reduction in the toxicity of the compounds.

Indolesulfonamides bind at the colchicine site

The study of the binding mode of the indolesulfonamides to the colchicine site has been accomplished by means of docking simulations. Subsequently, molecular dynamics simulations have been carried out for the complexes of the most potent analogues **5**, **9**, and **16** to confirm the stability of the proposed docking poses.

The docking process has been divided into two steps. First, flexible ligand docking was performed with two completely different scoring functions (PLANTS and AutoDock) to mitigate the inherent limitations of docking calculations⁶¹. Protein flexibility was accounted for by using an ensemble docking⁶² approach with all the available X-ray structures of colchicine site ligands in complex with tubulin²⁷ along with five representative structures from a previous molecular dynamics simulation¹⁹. For each ligand, the higher scored binding mode common to the two programs was considered as the consensus binding mode. We have validated this approach by analysing the docking of the ligands with known X-ray structures when in complex with the colchicine site of tubulin: the procedure retrieved in all but one case (corresponding to the covalently modified adduct of 3HKE) the observed configuration (RMSD < 2 Å) and in most cases corresponded to the first (52 out of 62) or second (8 out of 62) picks, with the software combination outperforming the individual performances. Furthermore, in most cases, the selected poses do not correspond to the self-docking pose (docking to the same pdbID of the X-ray structure) but other proteins are preferred (cross-docking), thus validating the use of multiple protein structures (ensemble docking approach).

Subsequently, the protein models yielding the higher number of consensus poses were selected for the comparison of the scorings of the different ligands in their consensus binding modes in an attempt to minimise the energetic contribution of the protein-energy changes due to configurational differences. The ligands (Figure 4) consistently adopt a *cisoid* conformation and occupy zone A with the trimethoxyphenyl, 3,5-dimethoxyphenyl, and 2,5-dimethoxyphenyl rings and zone B with the *N*-methylindole ring (corresponding to the trimethoxyphenyl and 3-hydroxy-4-methoxyphenyl rings of CA-4, respectively), as previously found for related combretastatins and isocombretastatin analogues. The methoxylated phenyl rings bind within the β subunit at the C-terminus of helix H7, contacting Cys241 β , the N-terminus of helix H8, contacting Leu255 β , and the H7-H8 loop, contacting Leu248 β and A250 β with the sulfonamide substituents and are boxed by sheets S9 (Lys352 β and Ala354 β), S8 (Ala316 β and Val318 β), and S10 (Ile378 β) that surround the methoxy groups. The indole rings bind at the N-terminus of helix H8 (Leu255 β , Asn258 β , and Met259 β), sheets S9 (Lys352 β), S8 (Thr314 β and Ala316 β) of the β subunit, with the indole 3-substituents pointing towards the α subunit (Ser178 α and Thr179 α). The substituents on the sulfonamide nitrogen point towards the interfacial surface of the tubulin subunits and occupy small hydrophobic sub-pockets, thus explaining the preference for the smaller substituents, such as the methyl or ethyl groups, over the free sulfonamide that places the polar N-H vector in a highly hydrophobic pocket or larger

Table 3. clogP, Area and Polar Surface Area (PSA) parameters were predicted with Spartan software.

No.	clogP	Area	PSA	% PSA/A	Δ relE
4	2.45	387.33	62.69	16.19	2.79
5	2.69	404.95	50.16	12.39	10.30
6	3.03	424.45	49.31	11.62	10.91
7	2.56	478.87	71.30	14.89	13.43
8	1.96	437.42	84.08	19.22	14.30
9	2.78	425.59	64.83	15.23	8.00
10	2.59	404.96	61.62	15.22	3.41
11	3.16	444.49	49.28	11.09	6.90
12	1.43	409.59	75.97	18.55	3.83
13	1.67	425.15	63.58	14.95	12.38
14	2.01	447.46	63.65	14.22	12.02
15	2.18	406.64	76.99	18.93	4.38
16	2.41	424.25	64.52	15.21	11.40
17E	2.93	456.41	64.52	14.14	11.24
17Z	2.93	453.44	64.53	14.23	10.80
18E	3.26	477.50	64.62	13.53	>25.57
18Z	3.26	475.27	64.65	13.60	15.28
21	2.58	357.56	58.05	16.23	2.65
22	2.82	373.37	45.62	12.22	10.04
23	3.15	397.26	45.71	11.51	10.71
24	2.68	446.04	67.42	15.11	13.06
25	2.91	398.38	61.24	15.37	10.15
26	4.55	458.44	44.21	9.64	11.10
27	4.71	464.39	44.14	9.51	11.95
28	1.17	391.36	95.56	24.42	3.50
29	1.80	396.75	60.56	15.26	10.90
30	3.53	481.58	59.11	12.27	13.15
31	2.54	395.84	60.92	15.39	11.16
32	4.27	479.60	59.60	12.43	12.92
35	2.58	358.72	57.07	15.91	1.99
36	2.82	376.11	43.67	11.61	7.22
37	2.68	444.48	64.09	14.42	11.22
38	2.91	397.98	59.85	15.04	4.26
39	4.55	457.86	42.93	9.38	4.60
40	1.56	382.52	71.40	18.67	2.75
41	1.80	397.77	57.99	14.58	6.37
42	2.30	381.13	72.45	19.01	3.44
43	2.25	418.32	72.69	17.38	1.12
44E	2.82	413.71	72.43	17.51	6.78
44Z	2.82	409.67	72.48	17.69	4.50
45	3.54	398.25	56.61	14.22	2.39
46	3.78	415.16	43.19	10.40	6.62
47	2.39	400.97	71.63	17.86	2.83
48	2.62	416.93	57.55	13.80	5.92
49	3.13	399.00	71.99	18.04	3.11
CA-4	3.33	349.20	43.40	12.43	
ABT-751	2.29	378.91	87.99	23.22	

Δ relE indicates the difference or relative energy between the *cisoid* and the *transoid* conformers with the least energy in kJ/mol. Conformer distribution analysis was performed with Spartan software.

substitutions that exceed the empty volume. The substituents at the indole 3-position point towards a polar region of the α subunit with threonine and serine sidechains, thus explaining the preference for hydrogen bond acceptor groups. Molecular dynamics simulations of the complexes of **5**, **9**, and **16** showed stable configurations along the trajectories, thus confirming the stability of the proposed docking poses (Supplemental Figure 2, SF2). Little correlation was found between the docking scores (Supplemental Table ST3) and the TPI or anti-proliferative IC₅₀s, reflecting the usual limitations found in docking campaigns. The most remarkable differences occur for larger ligands but attempts to replace the crude scorings by ligand efficiency measures did not improve on the results. Furthermore, the docking scores were unable to reproduce the relative potencies of the A ring variations and did not favour the observed preference found in the activity assays for the 3,4,5-trimethoxyphenyl ring. Even so, just considering a single protein configuration improved the predictive value of the

scores and reproduced the difficulties in introducing bulky substituents, as they bound in a non-preferred disposition. This selection of a single protein configuration was supported by re-scoring the docking poses with an MMGBSA approximation after short molecular dynamics runs that showed significant energy differences between different protein configurations that could make the comparison between poses docked to different proteins less significant.

Indolesulfonamides preferentially adopt a cisoid conformation

The conformational preference in sulfonamides is a relevant factor that contributes to the potency, as the docking results show binding in a *cisoid* disposition of the sulfonamide bridge. Considering that such conformational issues might not be well accounted for by the docking scoring functions, we performed DFT calculations of the conformational preferences of the ligands, quantified as the energy differences (Δ relE) between the *transoid* and *cisoid* conformations (Table 3). The *cisoid* conformations are preferred over the *transoid* ones, thus contributing to a higher binding affinity with tubulin. Substituents at the sulfonamide nitrogen increase, especially in 3,4,5-trimethoxyphenyl and 3,5-dimethoxyphenyl series (Table 3), the energy difference. The changes of the conformational equilibrium might be associated with the different potencies of the ligands and with the low correlation between docking and activity data.

Indole substitution increases polar surface area in indolesulfonamides

The replacement of the phenolic B ring of colchicine site ligands by indoles has been shown to increase potency but at the expense of higher lipophilicity that is associated with poor pharmacokinetics, with lower solubility and higher unspecific toxicity²⁵. To assess the effect of the introduced structural modifications here explored on their pharmacokinetics we have calculated relevant physicochemical properties that are considered relevant to this outcome (Table 3), such as the total polar surface area, the percentage of polar surface, and the clogP. With respect to the combretastatins and the isocombretastatins, the sulfonamides show lower clogP values, even below 3 (2.45 for **4** and 2.58 for **21** and **35**), following Pfizer's optimal drug-like properties for reduced toxicity, and increase PSA values above the desired safety threshold of 75 Å²²⁵. The introduction of amide, aldehyde, nitrile, or propenenitrile groups at the indole ring results in higher PSA, surpassing 75 Å² in compounds **12**, **15**, and **28**. The same contribution was observed for ester and carboxylic acid substituents at the sulfonamide bridge. In this respect, these modified indolesulfonamides, such as the cyanoindoles **15** and **16**, represent an improvement with respect to more hydrophobic analogues such as **4** or **5**, despite a small potency reduction.

Conclusions

Indolesulfonamides are highly potent antimitotic compounds but are very hydrophobic, which is a potential source of unspecific toxicity. Trying to improve the polarity and thus reduce the potential toxicity, 45 new indolesulfonamides with structural modifications at the indole 3-position, the sulfonamide bridge, and the substitution pattern of the A ring, have been prepared and evaluated as anti-proliferative agents against four human tumour cell lines, showing high potencies in the sub-micromolar to nanomolar

range. Co-treatment with the indolesulfonamides and MDR inhibitors showed that the indolesulfonamides are not substrates of the MDR proteins, one of the more frequent ways exploited by tumours to develop resistance. The indolesulfonamides inhibit microtubular protein polymerisation *in vitro* and in cells, thus suggesting that they exert their anti-proliferative activity by inhibiting tubulin. Flow cytometry studies of the effect of the treatment of HeLa cells with the indolesulfonamides on the cell cycle populations at different time points and drug concentrations showed that the compounds cause an early arrest at the G₂/M phase of the cell cycle, consistent with a tubulin inhibitory mechanism, that is followed by an increase in apoptotic cell death as indicated by the subG₀/G₁ population in the cell cycle distributions. However, the effects of these active compounds did not seem to be specific for tumour cells, as non-tumorigenic HEK-293 cells show IC₅₀ values at the same range as in different tumour cells. In this regard, both tumour and non-tumorigenic cells seem to be affected similarly by these indolesulfonamide drugs. However, it is interesting to note that the induction of the irreversible apoptotic response by these drugs in tumour cells versus non-tumorigenic cells differs. Thus, tumour cells were first arrested in G₂/M and then die by apoptosis following indolesulfonamide treatment. Non-tumorigenic tumour cells were also arrested in G₂/M upon treatment with the indolesulfonamide drugs, but the induction of apoptosis was lower and delayed. This delayed response to trigger an irreversible apoptotic cell death might result in a favourable reduction in the toxicity of the compounds, taking into account that the disruption of microtubules leading to cell cycle arrest could be reversible before the induction of apoptosis as previously described⁶³ and could hypothetically lead to a dormancy state of the tumour.

The most potent anti-proliferative agents were the *N*-methylated sulfonamides with a 3,4,5-trimethoxyphenyl A ring. Nitrile substituents at the indole 3-position resulted in more polar compounds with minimal potency reduction and therefore represent promising new antimitotic indolesulfonamides. The calculated physicochemical properties indicate that 3-cyanoindolesulfonamides are more polar and foresee an improved pharmacokinetic profile.

Molecular modelling studies have established binding with tubulin at the colchicine site with the phenyl ring of the benzene-sulfonamide binding at zone B in the interfacial surface between the subunits of the colchicine site, with the *N*-phenyl ring binding at the zone A within the subunit, and with the sulfonamide nitrogen pointing towards a small hydrophobic pocket close to the interfacial region. In summary, our results show that indolesulfonamides are potent antimitotic agents able to inhibit tumour cell proliferation, and are not sensitive to MDR and that polar substitutions at the indole 3-position, such as cyano groups, result in an optimal combination of anti-proliferative potency and polarity that makes them interesting new anti-tumour drugs for further development.

Acknowledgements

We thank the people at Frigoríficos Salamanca S.A slaughterhouse for providing us with the calf brains and "Servicio General de Espectrometría de Masas" of the Universidad de Salamanca for equipment. A.V.B. acknowledges a predoctoral fellowship from the Spanish Ministerio de Educación, Cultura y Deporte (FPU15/02457). M.G. acknowledges a predoctoral fellowship from the Junta de Castilla y León (ORDEN EDU/529/2017 de 26 de junio). A.V.B. thanks the Spanish Society of Medicinal Chemistry (SEQT)

for the “Ramón Madroño” award in the XIX Call for Prizes for Novel Researchers in Medicinal Chemistry.

Disclosure statement

The authors declare that they have no known competing financial interests of personal relationships that could have appeared to influence the work reported in this paper.

Funding

This work was financially supported by the Consejería de Educación de la Junta de Castilla y León [SA262P18 and SA116P20], co-funded by the EU's European Regional Development Fund-FEDER, and the Spanish Ministry of Science, Innovation, and Universities [RTI2018-099474-B-I00 and SAF2017-89672-R].

References

- Dumontet C, Jordan MA. Microtubule-binding agents: a dynamic field of cancer therapeutics. *Nat Rev Drug Disc* 2010;9:790–803.
- Vicente-Blázquez A, González M, Álvarez R, et al. Antitubulin sulfonamides: the successful combination of an established drug class and a multifaceted target. *Med Res Rev* 2019;39:775–830.
- Mollinedo F, Gajate C. Microtubules, microtubule-interfering agents and apoptosis. *Apoptosis*. 2003;8:413–50.
- Matson DR, Stukenberg PT. Spindle poisons and cell fate: a tale of two pathways. *Mol Interv* 2011;11:141–50.
- Berrieman HK, Lind MJ, Cawkwell L. Do beta-tubulin mutations have a role in resistance to chemotherapy? *Lancet Oncol* 2004;5:158–64.
- Pérez-Pérez M-J, Priego E-M, Bueno O, et al. Blocking blood flow to solid tumors by destabilizing tubulin: an approach to targeting tumor growth. *J Med Chem* 2016;59:8685–711.
- Ravelli RBG, Gigant B, Curmi PA, et al. Insight into tubulin regulation from a complex with colchicine and a stathmin-like domain. *Nature* 2004;428:198–202.
- Álvarez R, Medarde M, Peláez R. New ligands of the tubulin colchicine site based on X-ray structures. *Curr Topics Med Chem* 2014;14:2231–52.
- Young SL, Chaplin DJ. Combretastatin A4 phosphate: background and current clinical status. *Expert Op Investigational Drugs* 2004;13:1171–82.
- Yoshino H, Ueda N, Nijima J, et al. Novel sulfonamides as potential, systemically active antitumor agents. *J Med Chem* 1992;35:2496–7.
- Yoshimatsu K, Yamaguchi A, Yoshino H, et al. Mechanism of action of E7010, an orally active sulfonamide antitumor agent: inhibition of mitosis by binding to the colchicine site of tubulin. *Cancer Res* 1997;57:3208–13.
- Luo Y, Hradil VP, Frost DJ, et al. ABT-751, a novel tubulin-binding agent, decreases tumor perfusion and disrupts tumor vasculature. *Anti-Cancer Drugs* 2009;20:483–92.
- Ma T, Fuld AD, Rigas JR, et al. A phase I trial and in vitro studies combining ABT-751 with carboplatin in previously treated non-small cell lung cancer patients. *Chemotherapy* 2012;58:321–9.
- Michels J, Ellard SL, Le L, et al. A phase IB study of ABT-751 in combination with docetaxel in patients with advanced castration-resistant prostate cancer. *Ann Oncol* 2010;21:305–11.
- Segreti JA, Brooks KA, Marsh KC, et al. Tumour-selective anti-vascular effects of the novel anti-mitotic compound A-318315: an in vivo rat regional haemodynamic study. *Clin Exp Pharmacol Physiol* 2010;37:636–40.
- Gupta AK, King SA, Lee EC, et al. Process for the preparation of cell proliferation inhibitors. US 6,710,185 B2; 2004.
- Maya ABS, Pérez-Melero C, Mateo C, et al. Further naphthyl-combretastatins. An investigation on the role of the naphthalene moiety. *J Med Chem* 2005;48:556–68.
- Álvarez R, Gajate C, Puebla P, et al. Substitution at the indole 3 position yields highly potent indolecombretastatins against human tumor cells. *Euro J Med Chem* 2018;158:167–83.
- Álvarez R, Puebla P, Díaz JF, et al. Endowing indole-based tubulin inhibitors with an anchor for derivatization: highly potent 3-substituted indolephenstatins and indoleisocombretastatins. *J Med Chem* 2013;56:2813–27.
- Medina JC, Roche D, Shan B, et al. Novel halogenated sulfonamides inhibit the growth of multidrug resistant MCF-7/ADR cancer cells. *Bioorg Med Chem Lett* 1999;9:1843–6.
- Medina JC, Shan B, Beckmann H, et al. Novel antineoplastic agents with efficacy against multidrug resistant tumor cells. *Bioorg Med Chem Lett* 1998;8:2653–6.
- Shan B, Medina JC, Santha E, et al. Selective, covalent modification of beta-tubulin residue Cys-239 by T138067, an anti-tumor agent with in vivo efficacy against multidrug-resistant tumors. *Proc Nat Acad Sci USA* 1999;96:5686–91.
- Hu L, Li Z, Wang Y, et al. Novel pyridinyl and pyrimidinylcarbazole sulfonamides as antiproliferative agents. *Bioorg Med Chem Lett* 2007;17:1193–6.
- Wang Y-M, Hu L-X, Liu Z-M, et al. N-(2,6-dimethoxy-pyridine-3-yl)-9-methylcarbazole-3-sulfonamide as a novel tubulin ligand against human cancer. *Clin Cancer Res* 2008;14:6218–27.
- Hughes JD, Blagg J, Price DA, et al. Physicochemical drug properties associated with in vivo toxicological outcomes. *Bioorg Med Chem Lett* 2008;18:4872–5.
- Aprile S, Del Grosso E, Tron GC, Grosa G. In vitro metabolism study of combretastatin A-4 in rat and human liver microsomes. *Drug Metabol Disp* 2007;35:2252–61.
- RCSB PDB: Homepage. Available from: <https://www.rcsb.org/> [last accessed 1 June 2020].
- Case DA, Cheatham TE, 3rd, Darden T, et al. The amber biomolecular simulation programs. *J Comput Chem* 2005;26:1668–88.
- Swiss PDB Viewer - Home. Available from: <https://spdbv.vital-it.ch/> [last accessed 26 April 2021].
- Marvin | ChemAxon. Available from: <https://chemaxon.com/products/marvin> [last accessed 26 April 2021].
- Raccoon | AutoDock — AutoDock. Available from: <http://autodock.scripps.edu/resources/raccoon> [last accessed 26 April 2021].
- ADT/AutoDockTools — AutoDock. Available from: <http://autodock.scripps.edu/resources/adt> [last accessed 26 April 2021].
- Forli S, Huey R, Pique ME, et al. Computational protein-ligand docking and virtual drug screening with the AutoDock suite. *Nat Protoc* 2016;11:905–19.

34. Morris GM, Huey R, Lindstrom W, et al. AutoDock4 and AutoDockTools4: automated docking with selective receptor flexibility. *J Comput Chem* 2009;30:2785–91.
35. Korb O, Stütze T, Exner TE. Empirical scoring functions for advanced protein-ligand docking with PLANTS. *J Chem Info Model* 2009;49:84–96.
36. KNIME Analytics Platform | KNIME. Available from: <https://www.knime.com/knime-analytics-platform> [last accessed 26 April 2021].
37. Berthold MR, Cebron N, Dill F, et al. KNIME: the Konstanz information miner. In: Preisach C, Burkhardt H, Schmidt-Thieme L, Decker R, eds. *Data analysis, machine learning and applications*. Berlin (Germany): Springer; 2008:319–26.
38. Sommer K, Friedrich N-O, Bietz S, et al. UNICON: a powerful and easy-to-use compound library converter. *J Chem Info Model* 2016;56:1105–11.
39. Pettersen EF, Goddard TD, Huang CC, Couch GS, et al. UCSF Chimera—a visualization system for exploratory research and analysis. *J Comput Chem* 2004;25:1605–12.
40. Cheminformatics Software | Molecular Modeling Software | OpenEye Scientific. Available from: <https://www.eyesopen.com/> [last accessed 26 April 2021].
41. García-Pérez C, Peláez R, Therón R, López-Pérez LJ. JADOPPT: java based AutoDock preparing and processing tool. *Bioinformatics* 2017;33:583–5.
42. Graves AP, Shivakumar DM, Boyce SE, et al. Rescoring docking hit lists for model cavity sites: predictions and experimental testing. *J Mol Biol* 2008;377:914–34.
43. Allen WJ, Balius TE, Mukherjee S, et al. DOCK 6: impact of new features and current docking performance. *J Comput Chem* 2015;36:1132–56.
44. Case DA, Darden TA, Cheatham TE, et al. AMBER 11, University of California, San Francisco; 2010.
45. Hornak V, Abel R, Okur A, et al. Comparison of multiple Amber force fields and development of improved protein backbone parameters. *Proteins* 2006;65:712–25.
46. Lindorff-Larsen K, Piana S, Palmo K, et al. Improved side-chain torsion potentials for the amber ff99SB protein force field. *Proteins* 2010;78:1950–8.
47. Wang J, Wolf RM, Caldwell JW, Kollman PA, et al. Development and testing of a general amber force field. *J Comput Chem* 2004;25:1157–74.
48. Oelschlaeger P, Klahn M, Beard WA, et al. Magnesium-cationic dummy atom molecules enhance representation of DNA polymerase beta in molecular dynamics simulations: improved accuracy in studies of structural features and mutational effects. *J Mol Biol* 2007;366:687–701.
49. Joung IS, Cheatham TE. Determination of alkali and halide monovalent ion parameters for use in explicitly solvated biomolecular simulations. *J Phys Chem B* 2008;112:9020–41.
50. Joung IS, Cheatham TE. Molecular dynamics simulations of the dynamic and energetic properties of alkali and halide ions using water-model-specific ion parameters. *J Phys Chem B* 2009;113:13279–90.
51. Jorgensen WL, Jenson C. Temperature dependence of TIP3P, SPC, and TIP4P water from NPT Monte Carlo simulations: seeking temperatures of maximum density. *J Comput Chem* 1998;19:1179–86.
52. Humphrey W, Dalke A, Schulten K. VMD: visual molecular dynamics. *J Mol Graphics* 1996;14:33–38. 33–38.
53. Visual Molecular Dynamics. Available from: <http://www.ks.uiuc.edu/Research/vmd/> [last accessed 15 July 2021].
54. Vilsmeier A, Haack A. Über die einwirkung von halogenphosphor auf alkyl-formanilide. Eine neue methode zur darstellung sekundärer und tertiärer p -alkylamino-benzaldehyde. *Berichte Der Deutschen Chemischen Gesellschaft* 1927;60: 119–22.
55. Álvarez C, Álvarez R, Corchete P, et al. Diarylmethyloxime and hydrazone derivatives with 5-indoyl moieties as potent inhibitors of tubulin polymerization. *Bioorg Med Chem* 2008; 16:5952–61.
56. Álvarez C, Álvarez R, Corchete P, et al. Naphthylphenstatins as tubulin ligands: synthesis and biological evaluation. *Bioorg Med Chem* 2008;16:8999–9008.
57. Pindur U, Kim M-H. First reactions of vinylindoles with diethyl mesoxalate, nitrosobenzene, and chlorosulfonyl isocyanate: new functionalized and [b]annellated indoles. *Tetrahedron* 1989;45:6427–38.
58. Li L, Jiang S, Li X, et al. Recent advances in trimethoxyphenyl (TMP) based tubulin inhibitors targeting the colchicine binding site. *Euro J Med Chem* 2018;151:482–94.
59. González M, Ovejero-Sánchez M, Vicente-Blázquez A, et al. Methoxy and bromo scans on N-(5-methoxyphenyl) methoxybenzenesulfonamides reveal potent cytotoxic compounds, especially against the human breast adenocarcinoma MCF7 cell line. *J Enzyme Inhib Med Chem* 2021;36:1029–47.
60. Kavallaris M. Microtubules and resistance to tubulin-binding agents. *Nat Rev Cancer* 2010;10:194–204.
61. Charifson PS, Corkery JJ, Murcko MA, Walters WP. Consensus scoring: a method for obtaining improved hit rates from docking databases of three-dimensional structures into proteins. *J Med Chem* 1999;42:5100–9.
62. Amaro RE, Baudry J, Chodera J, Demir Ö, et al. Ensemble docking in drug discovery. *Biophys J* 2018;114:2271–8.
63. Laskowski RA, Swindells MB. LigPlot+: multiple ligand-protein interaction diagrams for drug discovery. *J Chem Info Model* 2011;51:2778–86.
64. Gajate C, Barasoain I, Andreu JM, Mollinedo F. Induction of apoptosis in leukemic cells by the reversible microtubule-disrupting agent 2-methoxy-5-(2',3',4'-trimethoxyphenyl)-2,4,6-cycloheptatrien-1-one: protection by Bcl-2 and Bcl-X(L) and cell cycle arrest. *Cancer Res* 2000;60:2651–9.